GEOTECHNICAL ENGINEERING

LUNAR SURFACE ENGINEERING PROPERTIES EXPERIMENT DEFINITION

FINAL REPORT: VOLUME IV OF IV
FLUID CONDUCTIVITY OF LUNAR SURFACE MATERIALS

by

F. C. HURLBUT
D. R. WILLIS
P. A. WITHERSPOON
C. R. JIH
P. RAGHURAMAN

PREPARED FOR GEORGE C. MARSHALL SPACE FLIGHT CENTER
HUNTSVILLE, ALABAMA, UNDER NASA CONTRACT NAS 8-21432

JULY 1971

SPACE SCIENCES LABORATORY

UNIVERSITY OF CALIFORNIA · BERKELEY

Space Sciences Laboratory
University of California
Berkeley, California 94720

LUNAR SURFACE ENGINEERING PROPERTIES EXPERIMENT DEFINITION

FINAL REPORT: VOLUME IV OF IV

FLUID CONDUCTIVITY OF LUNAR SURFACE MATERIALS

by

F. C. Hurlbut
D. R. Willis
P. A. Witherspoon
C. R. Jih
P. Raghuraman

Prepared for Marshall Space Flight Center,
Huntsville, Alabama, under NASA Contract
NAS 8-21432.

Control Number DCN 1-X-80-00058 S1 (IF)

July 1971

Space Sciences Laboratory Series 11 Issue 51

This report was prepared by the University of California, Berkeley, under Contract Number NAS 8-21432, Lunar Surface Engineering Properties Experiment Definition, for the George C. Marshall Space Flight Center of the National Aeronautics and Space Administration. This work was administered under the technical direction of the Space Sciences Laboratory of the George C. Marshall Space Flight Center.

PREFACE

This report presents the results of studies conducted during the period July 19, 1969 — July 19, 1970, under NASA Research Contract NAS 8-21432, "Lunar Surface Engineering Properties Experiment Definition." This study was sponsored by the Lunar Exploration Office, NASA Headquarters, and was under the technical cognizance of Dr. N. C. Costes, Space Science Laboratory, George C. Marshall Space Flight Center.

The report reflects the combined effort of five faculty investigators, a research engineer, a project manager, and eight graduate research assistants, representing several engineering and scientific disciplines pertinent to the study of lunar surface material properties. James K. Mitchell, Professor of Civil Engineering, served as Principal Investigator and was responsible for those phases of the work concerned with problems relating to the engineering properties of lunar soils and lunar soil mechanics. Co-investigators were William N. Houston, Assistant Professor of Civil Engineering, who was concerned with problems relating to the engineering properties of lunar soils; Richard E. Goodman, Associate Professor of Geological Engineering, who was concerned with the engineering geology and rock mechanics aspects of the lunar surface; Paul A. Witherspoon, Professor of Geological Engineering, who was concerned with fluid conductivity of lunar surface materials in general; Franklin C. Hurlbut, Professor of Aeronautical Science, who was concerned with experimental studies on fluid conductivity of lunar surface materials; and D. Roger Willis, Associate Professor of Aeronautical Science, who conducted theoretical studies on fluid conductivity of lunar surface materials. Dr. Karel Drozd, Assistant Research Engineer, performed laboratory tests and analyses pertinent to the development of a borehole jack for determination of the in situ characteristics of lunar soils and rocks; he also helped in the design of the borehole jack. H. Turan Durgunoglu, H. John Hovland, Laith I. Namiq, Parabaronen Raghuraman, James B. Thompson, Donald D. Treadwell, C. Robert Jih, Suphon Chirapuntu, and Tran K. Van served as Graduate Research Assistants and carried out many of the studies leading to the results presented in this

report. Ted S. Vinson, Research Engineer, served as project manager until May 1970, and contributed to studies concerned with lunar soil stabilization. H. John Hovland served as project manager after May 1970, and contributed to studies concerned with soil property evaluation from lunar boulder tracks.

Ultimate objectives of this project were:

1) Assessment of lunar soil and rock property data using information obtained from Lunar Orbiter, Surveyor, and Apollo missions.

2) Recommendation of both simple and sophisticated in situ testing techniques that would allow determination of engineering properties of lunar surface materials.

3) Determination of the influence of variations in lunar surface conditions on the performance parameters of a lunar roving vehicle.

4) Development of simple means for determining the fluid conductivity properties of lunar surface materials.

5) Development of stabilization techniques for use in loose, unconsolidated lunar surface materials to improve the performance of such materials in lunar engineering application.

The scope of specific studies conducted in satisfaction of these objectives is indicated by the following list of contents from the Detailed Final Report which is presented in four volumes. The names of the investigators associated with each phase of the work are indicated.

VOLUME I

MECHANICS, PROPERTIES, AND STABILIZATION OF LUNAR SOILS

1. Lunar Soil Simulant Studies
W. N. Houston, L. I. Namiq, J. K. Mitchell, and D. D. Treadwell

2. Determination of In Situ Soil Properties Utilizing an Impact Penetrometer
J. B. Thompson and J. K. Mitchell

3. Lunar Soil Stabilization Using Urethane Foamed Plastics
T. S. Vinson, T. Durgunoglu, and J. K. Mitchell

4. Feasibility Study of Admixture Soil Stabilization with Phenolic Resins
T. Durgunoglu and J. K. Mitchell

VOLUME II

MECHANICS OF ROLLING SPHERE-SOIL SLOPE INTERACTION
H. J. Hovland and J. K. Mitchell

1. Introduction

2. Analysis of Lunar Boulder Tracks

3. Model Studies of the Failure Mechanism Associated with a Sphere Rolling Down a Soil Slope

4. Pressure Distribution and Soil Failure Beneath a Spherical Wheel in Air-Dry Sand

5. Theoretical Studies

6. Rolling Sphere Experiments and Comparison with Theoretical Predictions

7. Utilization of Developed Theory

8. Conclusions and Recommendations

VOLUME III

BOREHOLE PROBES

1. Summary of Previous Work
R. E. Goodman, T. K. Van, and K. Drozd

2. An Experimental Study of the Mechanism of Failure of Rocks Under Borehole Jack Loading
T. K. Van and R. E. Goodman

3. A Borehole Jack for Deformability, Strength, and Stress Measurements in a 2-inch Borehole
R. E. Goodman, H. J. Hovland, and S. Chirapuntu

VOLUME IV

FLUID CONDUCTIVITY OF LUNAR SURFACE MATERIALS

1. Studies on Fluid Conductivity of Lunar Surface Materials — Theoretical Studies
P. Raghuraman and D. R. Willis

2. Studies on Fluid Conductivity of Lunar Surface Materials — Experimental Studies
F. C. Hurlbut, C. R. Jih, and P. A. Witherspoon

VOLUME IV CONTENTS

Page

PREFACE iii

CHAPTER 1. THEORETICAL STUDIES 1-1
P. Raghuraman and D. R. Willis

INTRODUCTION 1-1
FREE MOLECULE TIME CONSTANT OF DEAD-END PORES 1-2
Formulation and Assumptions 1-2
Upper Limit to the Time Constant 1-6
Lower Bound to the Time Constant 1-15
Conclusions 1-19
APPLICATION OF SUDDEN FREEZE MODEL TO POROUS MEDIA 1-20
Formulation and Assumptions. 1-20
CONCLUSIONS 1-25
APPENDIX 1-26
SYMBOLS 1-42

CHAPTER 2. EXPERIMENTAL STUDIES 2-1
F. C. Hurlbut, C. R. Jih, and P. A. Witherspoon

INTRODUCTION 2-1
BACKGROUND 2-1
DESIGN AND CONSTRUCTION OF APPARATUS 2-3
Introduction 2-3
Description of the Apparatus 2-3
SPECIMEN PREPARATION 2-8
PRELIMINARY OBSERVATIONS 2-10
CONTINUING PROGRAM 2-11

VOLUME IV

Studies on Fluid Conductivity of Lunar Surface Materials

Chapter 1. THEORETICAL STUDIES

P. Raghuraman and D. R. Willis

INTRODUCTION

Theoretical studies on the problem of developing a probe capable of measuring the fluid conductivity of porous media under lunar conditions have been pursued in two principal directions. In the first place, we have examined some aspects of the fundamental question as to whether or not the probe can operate in quasi steady state conditions or whether it will be operated while various transient phenomena are still affecting the flow. A reasonable estimate of the time to establish steady state conditions appears necessary in view of the limitations on the maximum in situ testing time imposed — both by gas storage limitations and by the time an astronaut can devote to this experiment. With this in mind, we have considered the effect of dead end pores, which initially contain essentially no gas and act for some time as sinks for mass flow, when gas first flows down the main (through) pores. Clearly a truly steady flow cannot be established before there is pressure equilibrium between the dead end pore and the open pore. In the next section, the influence of the length-to-radius ratio on the time constant for filling up the dead end pores in the free molecular limit is considered.

In the second principal line of study, we have focused our efforts on evaluating the degree of sophistication necessary to analyse the flow through a porous media with vacumn as one boundary condition. We recognise that the flow, in general, would contain an initial region of continuum flow which would undergo a gradual transition to free molecular flow. In an effort to obtain rough estimates, a sudden freeze model is proposed. The third section contains the application of this model to various other models of the porous media.

FREE MOLECULE TIME CONSTANT OF DEAD-END PORES

Formulation and Assumptions

The unsteady Boltzmann equation is used to find the time constant for filling up a dead-end pore at zero pressure. The dead-end pore is visualized as a straight cylinder (Fig. 1-1), of radius "a" and length "ℓ", closed at one end. The problem is posed as the calculation of the time constant of such a cylinder at zero pressure, separated from an infinite reservoir of gas by a diaphragm, which is suddenly removed at some instant $t = 0$. An approximate scheme is formulated to determine the time constant for filling the cylinder, and the influence of the length of the cylinder on the time constant.

The basic assumptions made in the formulation are:

1. The flow is sufficiently rarefied that the effect of intermolecular collisions within the cylinder can be ignored compared to the effect of collisions with the boundary, i.e., the flow is free molecular.
2. The molecules that strike the walls undergo perfect accomodation.
3. There is no accumulation or ablation at the wall.
4. The boundary distribution functions are Maxwellian; that is, the infinite pocket of gas outside the cylinder has a Maxwellian distribution, as do the molecules reflecting from the cylinder wall.

Taking the mass balance on a unit area of the wall at axial distance z and time, t, the number flux $\zeta_c(z,t)$, from the cylindrical wall, is

$$\zeta_c(z,t) = \zeta_{ec}(z,t) + \zeta_{cc}(z,t) + \zeta_{bc}(z,t) \qquad (4\text{-}1)$$

while the number flux, $\zeta_b(r,t)$, per unit area from the back end at radius, r, and time, t, is

$$\zeta_b(r,t) = \zeta_{cb}(r,t) + \zeta_{eb}(r,t), \qquad (4\text{-}2)$$

where ζ_{ij} is the number flux from i to j, with subscripts b, c, and e representing the back end, the cylindrical wall, and the cylinder entrance,

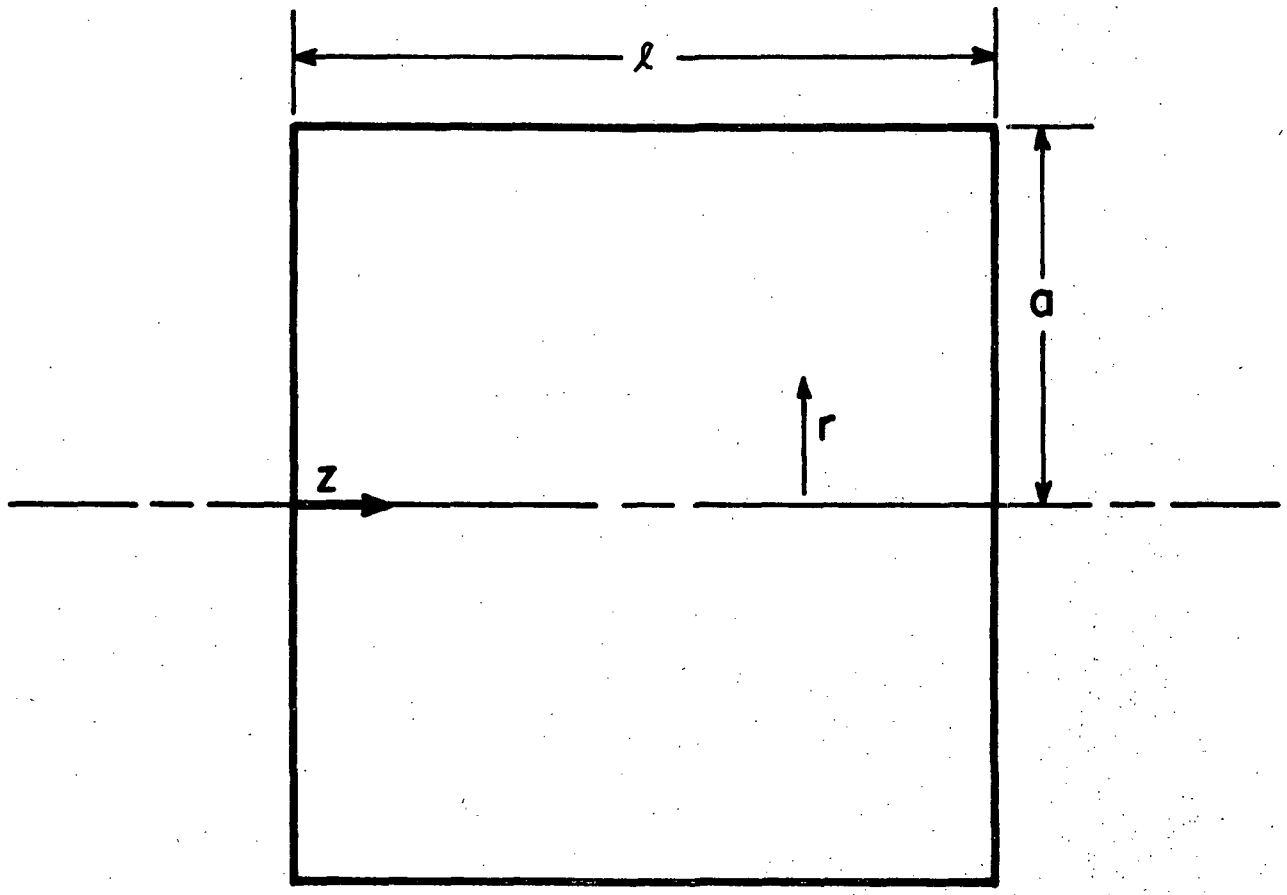

Fig. 1-1. Dead-end pore model

respectively. Also, the total outflux, e(t), from the cylinder at time t is

$$e(t) = e_c(t) + e_b(t), \tag{4-3}$$

where e_i is the number flux to the cylinder exit from i.

Each of the terms on the righthand side of Equations (4-1), (4-2), and (4-3) are evaluated using the ray tracing technique. The calculations detailed in the Appendix yield the following equations for (4-1), (4-2), and (4-3), respectively:

$$\zeta_c(z,t) = \frac{n_e\left(2RT_e\right)^{\frac{1}{2}}}{\pi^{\frac{3}{2}}} \int_0^{\tan^{-1}(2a/z)} d\theta \sin^2\theta \left(1 + \left[\frac{z}{t\left(2RT_e\right)^{\frac{1}{2}}\cos\theta}\right]^2\right)$$

$$\times \left(1 - \frac{z^2\tan^2\theta}{4a^2}\right)^{\frac{1}{2}} \exp\left(-\left[\frac{z}{t\left(2RT_e\right)^{\frac{1}{2}}\cos\theta}\right]^2\right)$$

$$+ \frac{4a^3}{\pi}\int_0^{\pi} d\theta\left(1 + \cos\theta\right)^2 \int_0^{\ell} \frac{dz'}{\left[(z' - z)^2 + 2a^2(1 + \cos\theta)\right]^2}$$

$$\times \int_0^{\infty} dc\, c^3\, e^{-c^2}\, \zeta_c\left(z', t - \frac{\left[(z' - z)^2 + 2a^2(1 + \cos\theta)\right]^{\frac{1}{2}}}{c\left(2RT_w\right)^{\frac{1}{2}}}\right)$$

$$+ \frac{4(\ell - z)}{\pi}\int_0^{\pi} d\theta \int_0^{a} \frac{dr\, r\,(a + r\cos\theta)}{\left[(\ell - z)^2 + a^2 + r^2 + 2ar\cos\theta\right]^2}$$

$$\times \int_0^{\infty} dc\, c^3\, e^{-c^2}\, \zeta_b\left(r, t - \frac{\left[(\ell - z)^2 + a^2 + r^2 + 2ar\cos\theta\right]^{\frac{1}{2}}}{c\left(2RT_w\right)^{\frac{1}{2}}}\right)$$

with

$$\zeta_b(r,t) = \frac{n_e\left(2RT_e\right)^{\frac{1}{2}}}{\pi^{\frac{3}{2}}} \int_{\tan^{-1}\left(\frac{a-r}{\ell}\right)}^{\tan^{-1}\left(\frac{a+r}{\ell}\right)} d\theta \cos^2\theta \frac{\left(r^2 - a^2 + \ell^2 \tan^2\theta\right)}{2r\ell}$$

$$\times\left(1 + \frac{\ell^2}{t^2\ 2RT_e \cos^2\theta}\right) \exp\left(-\frac{\ell^2}{t^2\ 2RT_e \cos^2\theta}\right)$$

$$+ \frac{4a}{\pi}\int_0^{\pi}(a + r\cos\theta)\, d\theta \int_0^{\ell} \frac{dz'(\ell - z')}{\left[(\ell - z')^2 + a^2 + r^2 + 2ar\cos\theta\right]^2}$$

$$\times\int_0^{\infty} dc\ c^3\ e^{-c2}\ \zeta_c\left(z, t - \frac{\left[(\ell - z')^2 + a^2 + r^2 + 2ar\cos\theta\right]^{\frac{1}{2}}}{c\left(2RT_w\right)^{\frac{1}{2}}}\right) \tag{4-5}$$

and

$$e(t) = 8\ell^2 \int_0^a dr\ r \int_0^{\pi} d\theta \int_0^a \frac{dr'r'}{\left[\ell^2 + r^2 + r'^2 + 2r\,r'\cos\theta\right]^2}$$

$$\times\int_0^{\infty} dc\ c^3\ e^{-c^2}\ \zeta_b\left[r, t - \frac{\left(\ell^2 + r^2 + r'^2 + 2r\,r'\cos\theta\right)^{\frac{1}{2}}}{c\left(2RT_w\right)}\right]$$

$$+ 8a\int_0^{\ell} dz\ z \int_0^a dr\ r \int_0^{\pi} \frac{d\theta(a + r\cos\theta)}{\left[z^2 + a^2 + r^2 + 2ar\cos\theta\right]^2}$$

$$\times\int_0^{\infty} dc\ c^3\ e^{-c^2}\ \zeta_c\left[z, t - \frac{\left(z^2 + a^2 + r^2 + 2ar\cos\theta\right)}{c\left(2RT_w\right)^{\frac{1}{2}}}\right] \tag{4-6}$$

where n_e and t_e are the number density and temperature outside the cylinder, Tw is the temperature of the inside surfaces, and c is molecular speed scaled by $\left(2RT_w\right)^{\frac{1}{2}}$.

We note that $\zeta_c(z,t)$, $\zeta_b(r,t)$ and e(t) are equal to zero for $t \leq 0$ while in the limit of larger values of t, they all tend to a constant value equal to $\left[n_e\left(2RT_e\right)^{\frac{1}{2}}\right]/2\pi^{\frac{1}{2}}$. Equations (4-4) and (4-5) constitute an integral equation for $\zeta_c(z,t)$. Once it is solved, $\zeta_b(r,t)$ and, hence e(t), can be easily determined from (4-5) and (4-6), respectively. The time constant is then determined as that value of time t at which e(t) reaches (1 - 1/e) of its final value $\left[n_e\left(2RT_e\right)^{\frac{1}{2}}\right]/2\pi^{\frac{1}{2}}$.

We will concern ourselves only with those situations wherein T_e and T_w do not differ appreciably. Then the only characteristic time in the filling of the cylinder is $\left[a/\left(2RT_e\right)^{\frac{1}{2}}\right]$, and the time constant will be equal to $A\left(\ell/a\right)\left[a/\left(2RT_e\right)^{\frac{1}{2}}\right]$. The problem as posed is to determine the function $A(\ell/a)$, which gives the dependence on (ℓ/a). In view of the motivation of this work, it does not seem appropriate to solve Equations (4-3), (4-4), and (4-5) in detail. Rather, a series of assumptions are made to yield simpler equations; these are then used to get the upper and lower bounds for the time constant as a function of the length-to-radius ratio, ℓ/a. In the next two subsections, the assumptions and the final equations for the upper and lower bounds are detailed.

Upper Limit to the Time Constant

The various assumptions made are:

1. The molecular velocity $C\left(2RT_w\right)^{\frac{1}{2}}$ involved in the time of flight occurring in the various number fluxes, is replaced by the most probable velocity $\left(2RT_w\right)^{\frac{1}{2}}$.
2. The center of the back end is taken as a typical and representative point for the back end.

These two assumptions lead to simplifications of the various terms involved on the righthand side of Equations (4-1), (4-2), and (4-3). The details are elaborated in the Appendix. The simplification for each term follows the derivation of the respective term.

3. The lengths of flights involved in the fluxes are square roots of expressions involving ℓ, a, r, θ, and z in various combinations. It is proposed to get rid of the square root and represent these lengths by "average" values.

Thus, in Equation (4-4), we represent $\left[(z - z')^2 + 2a^2(1 + \cos\theta)\right]^{\frac{1}{2}}$ averaged over θ by $|z' - z| + 2a/k$, with k, a function of $(|z - z'|)/a$, and $\left[(\ell - z)^2 + a^2 + r^2 + 2ar\cos\theta\right]^{\frac{1}{2}}$ at r = 0 (due to assumption 2) by $(\ell - z) + a/k_2$, where k_2 is a function of $(\ell - z')/a$. In Equation (4-5) we represent $\left[(\ell - z')^2 + a^2 + r^2 + 2ar\cos\theta\right]^{\frac{1}{2}}$ at r = 0 (due to assumption 2) by $(\ell - z') + a/k_2$ where r_2 is a function of $(\ell - z')/a$. Finally in Equation (4-6) we represent $\left[z^2 + a^2 + 2ar\cos\theta + r^2\right]^{\frac{1}{2}}$ averaged over θ and r by $z + 2a/k_3$ where k_3 is a function of z/a, and $\left[\ell^2 + r^2 + r'^2 + 2rr'\cos\theta\right]^{\frac{1}{2}}$ at r = 0 (due to assumption 2), averaged over r', by $\ell + a/k_4$ with k_4 as a function of ℓ/a. The last averaging is, however, valid only for large or "medium" length-to-radius ratios. For short length to radius ratios it is felt to be appropriate to represent the average of $\left(\ell^2 + r'^2\right)^{\frac{1}{2}}$ by ℓ itself.

Finally, we naively assume that $k_1 = k'_2 = k_3 = k_4 =$ a constant = k, say. This carries the tacit assumption that the exact values of k_1, k_2, k_3, and k_4 do not have a profound bearing on the final result.

The following scaling is introduced

$$\left.\begin{aligned}
\left[\frac{a/(Nk)}{\left(2RT_w\right)^{\frac{1}{2}}}\right] &= T \\
t/T &= J \\
z/\left(\frac{a}{Nk}\right) &= I \\
z'/\left(a/Nk\right) &= K \\
\ell/\left(a/Nk\right) &= LL \\
\left(\frac{T_w}{T_e}\right)^{\frac{1}{2}} &= m
\end{aligned}\right\} \quad (4\text{-}7a)$$

$$\left.\begin{aligned}
&\frac{\zeta_c(z,t)}{\left[n_e\left(2RT_e\right)^{\frac{1}{2}}/2(\pi)^{\frac{1}{2}}\right]} = F\left(\frac{a}{Nk}\, I,\ TJ\right)\\[2ex]
&\frac{\zeta_b(0,t)}{\left[n_e\left(2RT_e\right)^{\frac{1}{2}}/2(\pi)^{\frac{1}{2}}\right]} = F\left([LL+1]\,\frac{a}{Nk},\ TJ\right)\\[2ex]
&\left[\frac{e(t)}{\pi a^2}\right]\Big/\left[\frac{n_e\left(2RT_e\right)^{\frac{1}{2}}}{2(\pi)^{\frac{1}{2}}}\right] = E(TJ)
\end{aligned}\right\} \quad (4\text{-}7b)$$

The shorthand notation F(I,J), E(J), and F(LL + 1, J) are used for $F\left(\frac{a}{Nk}\, I,\ TJ\right)$, E(TJ), and $F\left[(LL+1)\,\frac{a}{Nk},\ TJ\right]$, respectively. The scaled flux from the back end has been called F(LL + i, J) for easier understanding of the mechanics of the problem.

If J,K, and I are taken as continous variables, then consequent to the three assumptions, Equations (4-4) through (4-6) take the following form:

$$F(I,J) = \frac{2}{\pi}\int_0^{\tan^{-1}\frac{2Nk}{I}} d\theta\, \sin^2\theta\left[1+\left(\frac{I\,m}{J\cos\theta}\right)^2\right]\ \exp\left[-\left(\frac{I\,m}{J\cos\theta}\right)^2\right]$$

$$\times\left(1-\frac{I^2\tan^2\theta}{4N^2k^2}\right)^{\frac{1}{2}} + \frac{1}{2Nk}\int_0^{LL} dk\left[1-\frac{|K-I|\left[(I-K)^2+6N^2k^2\right]}{\left[(I-K)^2+4N^2k^2\right]^{\frac{3}{2}}}\right]$$

$$\times F(K,\ J-|K-I|-2N) + \frac{(LL-I)}{2Nk}$$

$$\times\left[\frac{(LL-I)^2+2N^2k^2}{(LL-I)\left[(LL-I)^2+4N^2k^2\right]^{\frac{1}{2}}}-1\right] F(LL+1,\ J-LL+I-N) \quad (4\text{-}8)$$

with

$$F(LL + 1, J) = e^{-\left(\frac{LL}{J}\right)^2}\left[1 - \frac{e^{-\left(\frac{Nk}{J}\right)^2}}{\left(1 + \frac{N^2k^2}{LL^2}\right)}\right]$$

$$+ 2N^2k^2\int_0^{LL} \frac{dK(LL - K)}{\left[(LL - K)^2 + N^2k^2\right]^2} F(K, J - LL + K - N) \qquad (4\text{-}9)$$

and

$$E(J) = \frac{LL^2}{2N^2k^2}\left[\left(1 + \frac{2N^2k^2}{LL^2}\right) - \left(1 + \frac{4N^2k^2}{LL^2}\right)^{\frac{1}{2}}\right] F\left(LL + 1, J_1\right)$$

$$+ \frac{1}{N^2k^2}\int_0^{LL} dK\, K \left[\frac{K^2 + 2N^2k^2}{K\left(K^2 + 4N^2\right)^{\frac{1}{2}}} - 1\right] F(K, J - K - 2N\ , \qquad (4\text{-}10)$$

with

$J_1 = J - LL - N$ for large and moderate values of $\left(\frac{LL}{Nk}\right)$ and $J_1 = J - LL$ for small values of $\left(\frac{LL}{Nk}\right)$

For a numerical computation scheme, I, K, and J are taken as integers; while LL is always maintained as an even integer. The integrals in K can be represented as a sum with the integrand evaluated at odd values of K = 1, 3, 5 ... (LL - 1), so that dK = 2. However, this procedure had to be modified to account for the rapid variation in the kernels of some of

the integrals. Thus, in Equation (4-8), the conventional way of interpreting the second integral would be as

$$\frac{1}{Nk} \sum_{N=1,3}^{LL-1} \left\{ 1 - |K - I| \left[(K - I)^2 + 6N^2k^2 \right] / \left[(K - I)^2 + 4N^2k^2 \right]^{\frac{3}{2}} \right\}$$

$$\times F(K, J - |K - I| - 2N)$$

However, the kernel $\left\{ 1 - |K - I| \left[(K - I)^2 + 6N^2k^2 \right] / \left[(K - I)^2 + 4N^2k^2 \right]^{\frac{3}{2}} \right\}$ is a steeply varying function of K with a symmetry around $K = I$, where it has a maximum value of 1. The above summation is hence an overestimation. A more realistic interpretation would be to evaluate the kernal at $|K - I| = \frac{1}{2}$ rather than $K = I$, and hence represent the integral as equal to

$$\frac{1}{NR} \sum_{\substack{K=1,3... \\ K \neq I}}^{LL-1} \left\{ 1 - |K - I| \left[(K - I)^2 + 6N^2k^2 \right] / \left[(K - I)^2 + 4N^2k^2 \right]^{\frac{3}{2}} \right\}$$

$$\times F(K, J - |K - I| - 2N) + \frac{1}{Nk} \left[1 - \frac{(1 + 24N^2k^2)}{(1 + 16N^2k^2)^{\frac{3}{2}}} \right] F(I, J - 2N).$$

Further, in Equation (4-10), the terms

$$\left[\frac{K^2 + 2N^2k^2}{(k^2 + 4N^2k^2)^{\frac{1}{2}}} - K \right]$$

and $F(K, J - K - 2N)$, representing the integrand of the second term, are both functions that rapidly drop to negligible values as K increases. Designating the kernel

$$\frac{1}{N^2k^2} \left[\frac{K^2 + 2N^2k^2}{(K^2 + 4N^2k^2)^{\frac{1}{2}}} - K \right]$$

as P(K), and F(K, J - K - 2N) as g(K) (only space variation is of concern), the integral under examination, viz,

$$\int_0^{LL} ds\ P(s)\ g(s),$$

is interpreted as,

$$\sum_{K=1,3,\ldots}^{LL-1} \int_{(K-1)}^{K+1} ds\ P(s) \left[g(K) + g'(K)\ \frac{(S-K)}{2!} + g''(K)\ \frac{(S-K)^2}{2!} + \cdots \right],$$

where g(s) is expanded as a Taylor's series around S = K and g'(K), etc., are the derivatives with respect to S evaluated at K. Ignoring g" (K) and higher derivatives, and considering g'(K) only at K = 1, the integral under consideration is representable as

$$\sum_{K=1,3,\cdots}^{LL-1} \left\{ \frac{(K+1)}{2Nk} \left[\left(\frac{K+1}{Nk} \right)^2 + 4 \right]^{\frac{1}{2}} - \frac{(k-1)}{2Nk} \left[\left(\frac{K-1}{Nk} \right)^2 + 4 \right]^{\frac{1}{2}} - \frac{2K}{N^2k^2} \right\}$$

$$F(K, J-K-2N) + \left[F(3, J-3-2N) - F(I, J-1-2N) \right]$$

$$\times \frac{1}{3} \left[\left(\frac{1}{N^2k^2} - 2 \right) \left(1 + N^2k^2 \right)^{\frac{1}{2}} + \left(2Nk - \frac{1}{N^2k^2} \right) \right] .$$

Thus, Equations (4-8) through (4-10) take the following form:

$$F(I, J) = \frac{2}{\pi}\int_0^{\tan^{-1}\frac{2Nk}{I}} d\theta \sin^2\theta \left[1 + \left(\frac{I.m}{J\cos\theta}\right)^2\right] e^{-\left(\frac{I.m}{J\cos\theta}\right)^2} \left(1 - \frac{I^2\tan^2\theta}{4N^2k^2}\right)^{\frac{1}{2}}$$

$$+ \frac{1}{Nk}\sum_{\substack{K=1,3,-- \\ K\neq I}}^{LL-1} \left\{1 - \frac{|K - I|\left[(K - I)^2 + 6N^2k^2\right]}{\left[(K - I)^2 + 4N^2k^2\right]^{\frac{3}{2}}}\right\}$$

$$\times F(K, J - |K - I| - 2N) + \frac{1}{Nk}\left[1 - \frac{(1 + 24N^2k^2)}{\left(1 + 16N^2k^2\right)^{\frac{3}{2}}}\right] F(I, J - 2N)$$

$$+ \frac{(LL - I)}{2Nk}\left\{\frac{(LL - I)^2 + 2N^2k^2}{(LL - I)\left[(LL - I)^2 + 4N^2k^2\right]^{\frac{1}{2}}} - 1\right\}$$

$$\times F(LL + 1, J - LL + I - N) \qquad (4\text{-}11)$$

$$F(LL + 1, J) = e^{-\left(\frac{LL}{J}\right)^2}\left[1 - \frac{e^{-\left(\frac{Nk}{J}\right)^2}}{1 + \frac{N^2k^2}{LL^2}}\right] + 4N^2k^2\sum_{K=1,3,--}^{LL-1} \frac{(LL - K)}{\left[\left(LL - K\right)^2 + N^2k^2\right]^2}$$

$$F(K, J - LL + K - N) \qquad (4\text{-}12)$$

and

$$E(J) = \frac{1}{2}\left(\frac{LL}{Nk}\right)^2\left[\left(1 + \frac{2N^2k^2}{LL^2}\right) - \left(1 + \frac{4N^2k^2}{LL^2}\right)^{\frac{1}{2}}\right] F(LL + 1, J_1)$$

$$+ \frac{1}{3}\left\{F(3, J - 3 - 2N) - F(1, J - 1 - 2N)\right\} \times \left\{\left(\frac{1}{N^2k^2} - 2\right)\left(1 + N^2k^2\right)^{\frac{1}{2}}\right.$$

$$\left. + \left(2Nk - \frac{1}{N^2k^2}\right)\right\} + \sum_{K=1,3,--}^{LL-1} \left\{\frac{(K + 1)}{2Nk}\left(\frac{(K + 1)^2}{N^2k^2} + 4\right)^{\frac{1}{2}}\right.$$

$$\left. - \frac{(K - 1)}{2Nk}\left(\frac{(K - 1)^2}{N^2k^2} + 4\right) - \frac{2K}{Nk}\right\} F(K, J - K - 2N) \quad , \qquad (4\text{-}13)$$

where $J_1 = J - LL - N$ for large and moderate values of $\left(\frac{LL}{Nk}\right)$, while $J_1 = J - LL$ for small values of $\left(\frac{LL}{Nk}\right)$.

Equations (4-11) through (4-13) can be easily solved numerically by the process of "stepping forward in time." The first integral in Equation (4-11) is evaluated using a five-point Gaussian quadrature scheme. Due to the numerical finite difference quadratures [F(I, J), F(LL + 1, J), and E(J)] in the limit $J \to \infty$ do not tend to 1 as they should. They are hence forced to tend to 1 by using correction factors: HF(I), the correction factor for F(I, J), multiplies all terms on the right side of Equation (4-11) except the first integral: HB and HE, the correction factors for F(LL + 1, J) and E(J), respectively, multiply Equations (4-12) and (4-13), respectively, with

$$HF(I) = \frac{1 - \frac{2}{\pi}\int_0^{\tan^{-1}\frac{2Nk}{I}} d\theta \, \sin^2\theta\left(1 - \frac{I^2\tan^2\theta}{4N^2k^2}\right)^{\frac{1}{2}}}{\text{denominator}}$$

where

denominator:

$$\left\{\frac{(LL - I)}{2Nk}\left[\frac{(LL - I)^2 + 2N^2k^2}{(LL - I)\left[(LL - I)^2 + 4N^2k^2\right]^{\frac{1}{2}}} - 1\right] + \frac{1}{Nk}\left[1 - \frac{\left(1 + 24N^2k^2\right)}{\left(1 + 16N^2k^2\right)^{\frac{3}{2}}}\right]\right.$$

$$\left. + \frac{1}{Nk}\sum_{\substack{K=1,3,-- \\ K=I}}^{LL-1}\left(1 - \frac{|K - I|\left[(K - I)^2 + 6N^2k^2\right]}{\left[(K - I)^2 + 4N^2k^2\right]^{\frac{3}{2}}}\right)\right\} \qquad (4\text{-}14)$$

$$HB = \frac{1}{\left\{\frac{N^2k^2}{LL^2 + N^2k^2} + 4N^2k^2\sum_{K=1,3,--}^{LL-1}\frac{(LL - K)}{\left[(LL - K)^2 + N^2k^2\right]^2}\right\}} \qquad (4\text{-}15)$$

and

$$HE = \frac{1}{\text{denominator}}$$

where

denominator:

$$\left\{\frac{1}{2}\left(\frac{LL}{Nk}\right)^2\left[\left(1 + \frac{2N^2k^2}{LL^2}\right) - \left[1 + \frac{4N^2k^2}{LL^2}\right]^{\frac{1}{2}}\right\} + \sum_{K=1,3,--}^{LL-1}\left\{\frac{(K + 1)}{2Nk}\right.$$

$$\left.\left[\left(\frac{K + 1}{Nk}\right)^2 + 4\right]^{\frac{1}{2}} - \frac{(k - 1)}{2Nk}\left[\left(\frac{K - 1}{Nk}\right)^2 + 4\right]^{\frac{1}{2}}\right\} \cdot \qquad (4\text{-}16)$$

The time constant is determined as that value of J at which E(J) exceeds (1 - 1/e). Two computer programs were formulated; one to solve Equations (4-11) through (4-13) for large and moderate values of LL/Nk ranging from 24 to 1, while the second was used to solve the same equations for small values of LL/Nk ranging from 1 to 1/64. It is worthy of note that using finer and finer meshes by increasing N was not found to change results at all (increasing N is equivalent to taking finer meshes in space as also finer increments in time).

Figure 1-2 shows a plot of the time constant (upper bound) vs LL/Nk. Figure 1-3 shows an amplified plot of Figure 1-2 for small values of (LL/Nk).

Lower Bound to the Time Constant

The relevant equations are again (4-4) through (4-6), and the first two assumptions made for the upper bound are made here again. Assumption 3 for the upper bound case is still used, but the "averages" are deliberately underestimated. This is equivalent to underestimating the time of flights. Thus, in Equation (4-4) we represent the average over θ of

$$\left[(z' - z)^2 + 2a^2(1 + \cos\theta)\right]^{\frac{1}{2}}$$

by $|z' - z|$ and

$$\left[(\ell - z)^2 + a^2 + r^2 + 2ar\cos\theta\right]^{\frac{1}{2}}$$

at r = 0 (due to assumption 2) by $(\ell - z)$. In Equation (4-5) we represent

$$\left[(\ell - z')^2 + a^2 + r^2 + 2ar\cos\theta\right]^{\frac{1}{2}}$$

at r = 0 (by assumption 2) by $(\ell - z')$. Finally, in Equation (4-6), we represent

$$\left[z^2 + a^2 + r^2 + 2ar\cos\theta\right]^{\frac{1}{2}}$$

and

$$\left[\ell^2 + r^2 + r'^2 + 2rr'\cos\theta\right]^{\frac{1}{2}}$$

at r' = 0 (by assumption 2) averaged over θ and r by z and 1, respectively. Scaling is done as in Equation (4-7) with k now set equal to 1. In finite difference form, the resultant equations (after amendments of some of the integrand as in the case of the upper bound) are:

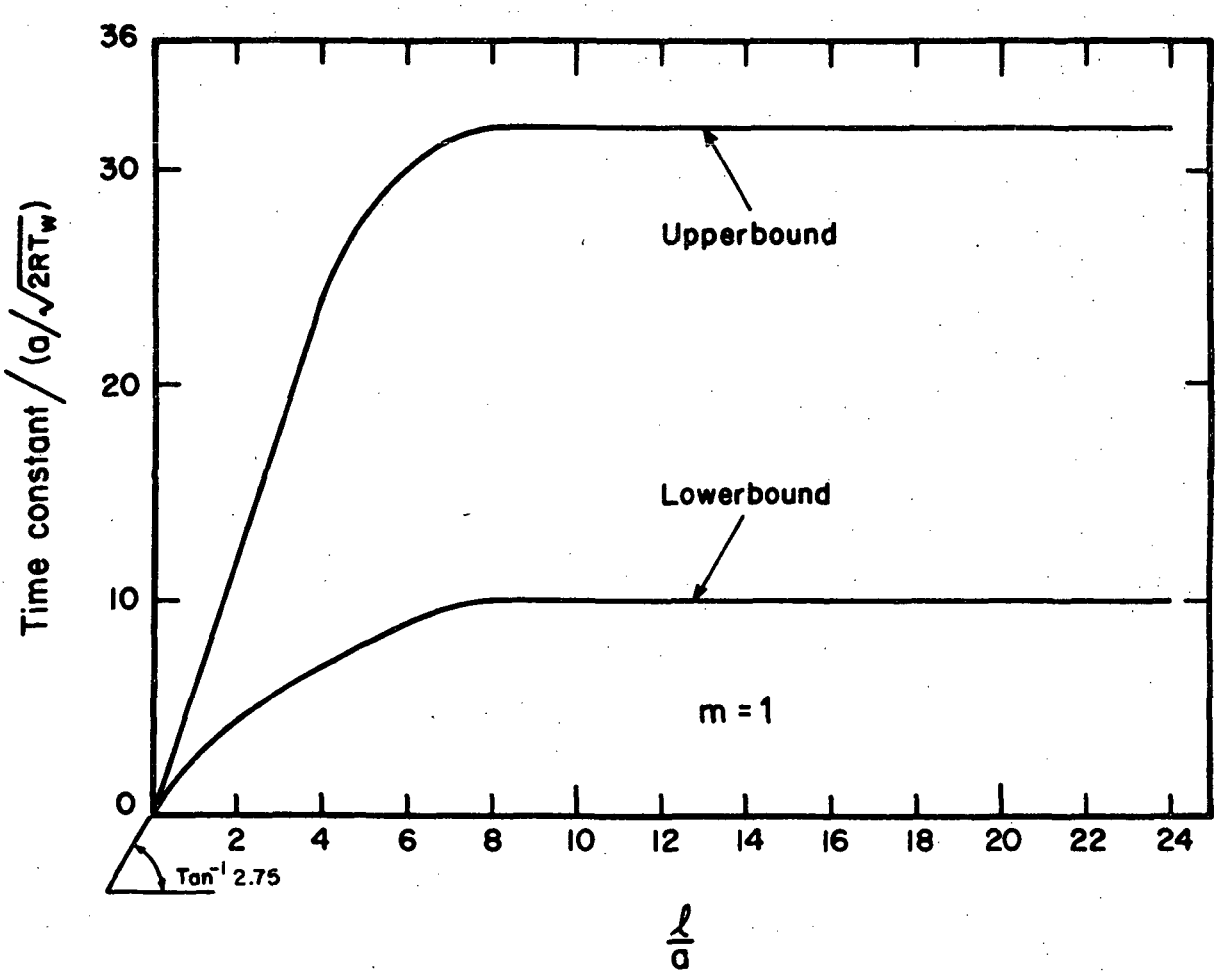

Fig. 1-2. Variation of time constant with length to radius ratio.

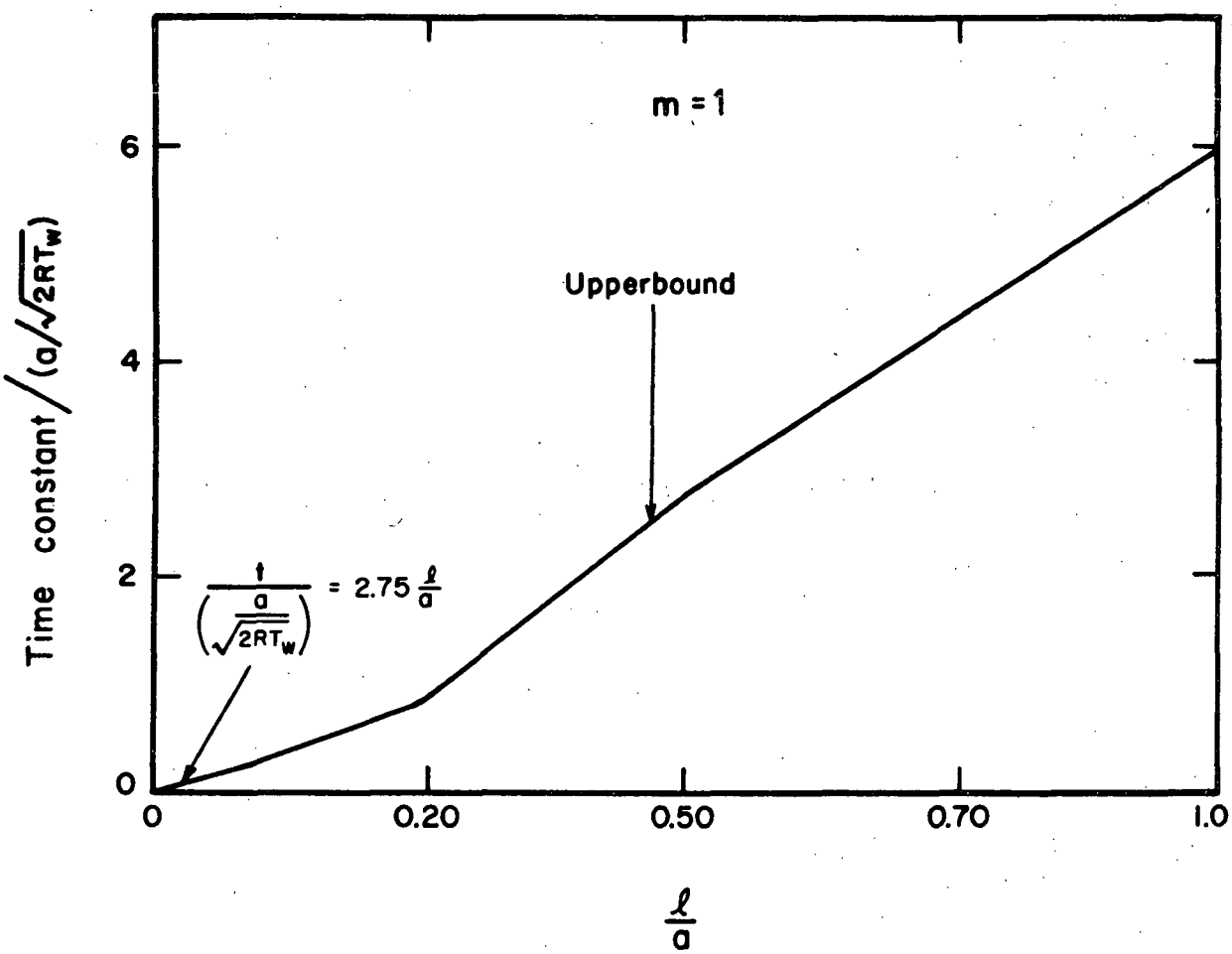

Fig. 1-3. Variation of time constant with small length to radius ratio.

$$F(I, J) = \frac{2}{\pi} \int_0^{\tan^{-1}\frac{2a}{I}} d\theta \, \sin^2\theta \left[1 + \left(\frac{I\,m}{J\cos\theta}\right)^2\right] e^{-\left(\frac{I\,m}{J\cos\theta}\right)^2}$$

$$\times \left(1 - \frac{I^2 \tan\theta}{4N^2}\right)^{\frac{1}{2}} + \frac{1}{N} \sum_{\substack{K=1,3,-- \\ K\neq I}}^{LL-1} \left\{1 - \frac{|K - I|\,(K - I)^2 + 6N^2}{\left[(K - I)^2 + 4N^2\right]^{\frac{3}{2}}}\right\}$$

$$\times F(K, J - |K - I|) + \frac{1}{N} \left[1 - \frac{(1 + 24N^2)}{(1 + 16N^2)^{\frac{3}{2}}}\right] F(I, J)$$

$$+ \frac{(LL - I)}{2N} \left\{\frac{(LL - I)^2 + 2N^2}{(LL-I)\left[(LL - I)^2 + 4N^2\right]^{\frac{1}{2}}} - 1\right\} F(LL + 1, J - LL + I) \cdot$$

(4-17)

$$F(LL + 1, J) = e^{-\left(\frac{LL}{J}\right)^2} \left[1 - \frac{e^{-\left(\frac{N^2}{J^2}\right)}}{1 + \frac{N}{LL^2}^2}\right]$$

$$+ 4N^2 \sum_{K=1,3,--}^{LL-1} \frac{(LL - K)}{\left[(LL - K)^2 + N^2\right]^2} F(K, J - LL + K) \cdot$$

(4-18)

$$E(J) = \frac{1}{2}\left(\frac{LL}{N}\right)^2 \left[1 + \frac{2N^2}{LL^2} - \left(1 + \frac{4N^2}{LL^2}\right)^{\frac{1}{2}}\right] F(LL + 1, J - LL)$$

$$+ \frac{1}{3}\left\{F(3, J - 3) - F(1, J - 1)\right\}\left\{\left(\frac{1}{N^2} - 2\right)\left[1 + N^2\right]^{\frac{1}{2}} + 2N - \frac{1}{N^2}\right\}$$

$$+ \sum_{K=1,3,--}^{LL-1} \left\{\frac{(K + 1)}{2N}\left[\frac{(K + 1)^2}{N^2} + 4\right]^{\frac{1}{2}} - \frac{(K - 1)}{2N}\left[\frac{(K - 1)^2}{N^2} + 4\right]^{\frac{1}{2}}\right.$$

$$\left. - \frac{2K}{N}\right\} F(K, J - K) \cdot$$

(4-19)

Correction factors HF(I), HE, HB from Equations (4-14) through (4-16) are used again. Another computer program was evolved to solve Equations (4-17) through (4-19), with the time constant being determined as that value of J at which E(J) exceeds (1 - 1/e). Figure 1-2 shows the plot of the time constant vs LL/Nk.

It bears observation that the time constant obtained is truly the lower bound since the length of flight, and hence the time of flight used, is the minimum possible (within the framework of assumptions 1 and 2). In fact, the time of flight between two elements $\left[\text{at a speed } \left(2RT_w\right)^{\frac{1}{2}}\right]$ is assumed to be equal to that of a particle moving parallel to the z axis. We hence have the anamoly that the speed of particles in the radial direction is infinite. However, we have achieved our objective — that of finding an upper and a lower bound to the time constant, although as evidenced from Figure 4-2, the span between the two bounds is rather large.

Conclusions

The plot of the time constant vs ℓ/a shows that the time constant tends to a constant as ℓ/a increases. This is directly attributable to the assumption of diffuse reflection from the wall wherein each wall element reflects to the exit a fraction of the flux coming to the element, whose value depends on the solid angle made by the wall element with the exit. Thus, while the time constant increases with ℓ/a for small ℓ/a, after a certain stage adding new wall elements (i.e., increasing the cylinder length) is not going to increase the time constant, since not only does the solid angle subtended by the wall element to the exit decrease rapidly (as axial distance from exit increases), but also the flux to the element (and hence flux from the element) is small in the time scales considered.

It is obvious that, if, the walls were specularly reflecting, the time constant will progressively increase with ℓ/a. Most surfaces are partly diffuse and partly specular reflecting, being more diffuse than specular in nature. It is hence possible to anticipate results similar to our results for real surfaces; however, the exact value to which the time constant tends, depends very much on the nature of the cylinder surface.

APPLICATION OF SUDDEN FREEZE MODEL TO POROUS MEDIA

Formulation and Assumptions

The degree of sophistication necessary to analyzing the flow through porous media with vacuum as one boundary condition is evaluated. It is recognised that the flow, in general, would contain an initial region of continuum flow that would undergo a gradual transition to free molecular flow. However, if the initial region of continuum flow prevails over a sufficiently large distance from the probe, the continuum equations can be used with very little loss of accuracy. In an effort to obtain rough estimates of the length of this continuum flow, a sudden freeze model is proposed. Such a flow model is applied to various models of the porous media.

The basic assumptions made here are:

1. The temperature T of the flow is constant.
2. The flow which is initially continuum undergoes transition to free molecular flow abruptly at a section termed "the freeze section." Properties at this section are described by the subscript "f." The freeze section is identified as one wherein the mean free path, λ, is equal to the pore radius, a.

First a one-dimensional flow through a slab of finite thickness ℓ is considered. The medium is visualised as being made up of a bundle of straight, capillary tubes of constant radius, a . Let the pressure at the entrance of the tube (i.e., at the probe) be p_1 and the pressure at the other end of tube be equal to 0. Let the freeze section at which the mean free path $\lambda = a$, have a pressure p_f and be at a length ℓ_f from entrance.

In the continuum section, the flow is a poiseuille flow. Hence the mass flux through each tube per unit time is

$$Q = - \rho \frac{\pi a^4}{8\mu} \frac{dp}{dx} , \qquad (4\text{-}20)$$

where μ is the viscosity, dp/dx the pressure gradient along the tube axis and x the coordinate along the tube axis. Integrating (4-20) with respect

to x from the entrance to the freeze section, we have (since $p = \rho RT$ and Q is a constant)

$$Q = \frac{\left(p_1^2 - p_f^2\right)}{16\mu\ RT\ \ell_f}\ \pi a^4 \quad . \tag{4-21}$$

Assuming $p_1 >> p_f$ we have

$$Q = \frac{p_1^2\ \pi a^4}{16\mu\ RT\ \ell_f} \quad . \tag{4-22}$$

In the free molecule region

$$Q = - C\ \frac{\frac{dp}{dx}}{\bar{V}}\ a\ \pi a^2 \tag{4-23}$$

where C is a constant of O(1) and $\bar{V} = \left(\frac{8RT}{\pi}\right)^{\frac{1}{2}}$.

Integrating (4-23) between the freeze section and the tube exit, we have

$$Q = \frac{C\ \pi a^3}{\bar{V}}\ \frac{p_f}{\left(\ell - \ell_f\right)} \quad . \tag{4-24}$$

Since at freeze section $\lambda = \lambda_f = \frac{2\mu}{\left(\frac{p_f}{RT}\right)\bar{V}} = a$,

hence substituting for p_f in (4-24) and equating (4-22) and (4-24) for Q, we have

$$\frac{\ell f}{\ell} = \left[1 + 8C\left(\frac{\lambda_1}{a}\right)^2\right]^{-1} \tag{4-25}$$

where

$$\lambda_1 = \frac{2\mu}{\bar{V}\left(\frac{p_1}{RT}\right)}$$

= mean free path at tube entrance (i.e., probe).

Next, a one-dimension spherically symmetric flow through a semi-infinite medium is considered. Let r_1 be the probe radius, and p_1 and λ, the pressure and mean free path at the probe. (Strictly, the end of the probe will probably not be a hemisphere, so r_1 should merely be regarded as a typical length seal for the tip of the probe). Let r_f be the freeze radius and p_f the pressure at the freeze radius. Let the pressure at infinity be zero. The porous medium is visualised as an assembly of isotropic, randomly oriented, straight cylindrical pores of constant radius "a", connected to one another at the ends. Several pores may start or finish at these end points.

In the continuum region the mass flux Q is given by Darcy's Law as

$$Q = -\varrho \frac{K}{\mu} \frac{dp}{dr} 2\pi r^2 \qquad (4\text{-}26)$$

where K is the permeability and r is the radius.

Integrating (4-26) between r_1 and r_f, we have (noting $\varrho = \frac{p}{RT}$ and that Q is a constant)

$$Q = \frac{\pi K}{\mu RT} \frac{\left(p_1^2 - p_f^2\right)}{\left(r_f - r_1\right)} r_f r_1 \qquad (4\text{-}27)$$

We now consider the free molecular region. Consider a point at radius r. The pores being randomly oriented, the number of tubes at radius r with angular orientations (spherical coordinates r, θ and ϕ) between θ and $\theta + d\theta$ and ϕ and $\phi + d\phi$ is

$$= \left(\frac{4\pi\ \alpha r^2}{\pi a^2}\right) \frac{\sin\theta\ d\theta\ d\phi}{4\pi}$$

$$= \frac{\alpha r^2}{\pi a^2} \sin\theta\ d\theta\ d\phi,$$

where α is the porosity of the porous medium.

Since, in the free molecule limit, the mass flux through each tube is

$$= - C \frac{\pi a^3}{\bar{v}} \cos\theta \frac{dp}{dr} .$$

hence the mass flux over a radius r in the outward direction (along increasing r) is

$$Q = \int_{\theta=0}^{\frac{\pi}{2}} \int_{\phi=0}^{2\pi} \left(d\theta \, d\phi \, \frac{\alpha r^2}{\pi a^2} \sin\theta \right) \left(- \frac{C\pi a^3}{\bar{v}} \cos\theta \frac{dp}{dr} \right)$$

$$= - \pi C \frac{\alpha}{\bar{v}} \frac{dp}{dr} r^2 . \qquad (4\text{-}28)$$

Integrating (4-28) (and noting that Q is a constant) between r_f and infinity, we have

$$Q = \pi C \alpha \frac{a r_f}{\bar{v}} p_f . \qquad (4\text{-}29)$$

Equating (4-27) and (4-29), assuming $p_1 >> p_f$ and using the fact that

$$\lambda_f = a = \frac{2\mu RT}{\bar{v} p_3} ,$$

we have

$$\frac{r_f}{r_0} = 1 + \frac{2K}{C \alpha \lambda_0^2}$$

$$= 1 + \frac{2M}{C \alpha} \left(\frac{\alpha}{\lambda_0} \right)^2 \qquad (4\text{-}30)$$

where we assume that $K = M a^2$ with M, a constant of O(1).

Finally a one-dimensional flow through a slab of thickness ℓ is considered, using the above random pore orientation model. The notations used are the same as for the case of parallel capillary tube with ℓ_f now denoting the section at which flow freezes.

In the continuum region, the mass flux Q per unit are given by Darcy's law as

$$Q = - \frac{\varrho K}{\mu} \frac{dp}{dx} ,$$

where x is the coordinate along the line joining the end faces of the slab.

Integrating the above equation between x = 0 (from probe) to the freeze section $x = \ell_f$ and using $\varrho = \frac{p}{RT}$ we have,

$$Q = \frac{K}{2\mu RT} \frac{\left(p_1^2 - p_3^2\right)}{\ell_f}$$

$$\simeq \frac{K}{2\mu RT} \frac{p_1^2}{\ell_f} \qquad \text{on assuming } p_1 >> p_3 . \tag{4-31}$$

Let us now consider the free molecule flow. Here at a section, x, the total number of tubes with angular orientations between θ and $\theta + d\theta$, ϕ and $\phi + d\phi$, per unit area is

$$= \frac{\alpha}{\pi a^2} \frac{\sin\theta}{4\pi} \, d\theta \, d\phi .$$

Mass flux through each tube

$$= - C \frac{\frac{dp}{dx} \pi a^3}{\bar{v}} \cos\theta .$$

Hence total mass flux Q per unit area at x is

$$Q = \int_{\theta=0}^{\frac{\pi}{2}} \int_{\phi=0}^{2\pi} \left(d\theta \, d\phi \, \sin\theta \, \frac{\alpha}{\pi a^2}\right) \left(- C \frac{dp}{dx} \frac{\pi a^3}{\bar{v}} \cos\theta\right)$$

$$= - \frac{a \, c \, \alpha}{4\bar{v}} \frac{dp}{dx} . \tag{4-32}$$

Integrating (4-32) with respect to x from $x = \ell_f$ to $x = \ell$ (and noting Q is a constant) we have

$$Q = \frac{\alpha C a}{4\bar{V}} \frac{p_f}{(\ell - \ell_f)} \tag{4-33}$$

Equating (4-31) and (4-33), and noting that $p_f = \frac{2\mu RT}{\bar{V}a}$ we have

$$\frac{\ell_f}{\ell} = \left[1 + \frac{\alpha C}{4M}\left(\frac{\lambda_1}{a}\right)^2\right]^{-1} , \tag{4-34}$$

where

$$\lambda_1 = \frac{2M}{\bar{V}\left(\frac{p_1}{RT}\right)}$$

= mean free path at tube entrance (i.e.,probe)

while we assume $K = Ma^2$ where M is a constant of O(1).

CONCLUSIONS

To summarize the results obtained, we have: For the one-dimensional slab flow using both the porous medium models, we find that the ratio of the freeze length to the total slab thickness is $\left[1 + O(1) \times \left(\lambda_1/a\right)^2\right]^{-1}$, where λ, is the mean free path of the gas at the probe entrance and a the pore radius. In the spherically semi-infinite flow, the ratio of the freeze radius to the probe radius is estimated as $\left[1 + O(1) \times \left(a/\lambda_1\right)^2\right]$.

On the basis of a moon grain size of 10^{-2} to 10^{-3} cm, the pore radius can be roughly gauged to be 10^{-3} to 10^{-4} cm. If, for example, nitrogen is pumped from the probe to the lunar surface at a pressure of about 1 atmosphere and normal (15° C) temperature, then $\lambda_1 >> a$, and transition will occur far from probe. Hence the continuum equations can be safely used. However for rocks of smaller pore size ($\leq 10^{-5}$ cms) λ_1 and a are of the same magnitude and transition will occur near the probe — a detailed analysis of the transition flow is called for in such a case.

APPENDIX

1. Formula for entrance to cylinder flux $\zeta_c(z, t)$

The initial value for the distribution function f at time t = 0 is

$$f = \frac{n_e}{\left(2\pi\ RT_e\right)^{\frac{3}{2}}} \exp\left(\frac{-\underline{\xi}\ \underline{\xi}}{2RT_e}\right) \delta(z), \text{ where } \underline{\xi} \text{ is the molecular velocity}$$

and $\delta(z)$ is a function such that

$$\delta(z) = 1 \quad \text{for } z \leq 0$$
$$= 0 \quad \text{for } z \geq 0 .$$

Solving the unsteady Boltzmann equation in the free molecular limit for the above initial value, we have

$$f_e(\underline{r}, \underline{\xi}, t) = f_e(z, \underline{\xi}, t) = \frac{n_e}{\left(2\pi\ RT_e\right)^{\frac{3}{2}}} \exp\left(\frac{-\underline{\xi}\ \underline{\xi}}{2RT_e}\right)\delta(z - \xi_z t) .$$

If $\underline{n}$ be the unit normal at the wall at z, the number flux from the entrance to an annulus of unit area located at the wall at z, at time t is

$$\zeta_{ec}(z, t) = \int d^3\underline{\xi}\ f_e(z, \underline{\xi}, t)\ \underline{\xi} \cdot \underline{n} .$$

Using a spherical coordinate system fixed to the wall as shown in Figure 1-A1, we have

$$\underline{\xi} \cdot \underline{n} = \xi \sin\theta \cos\phi .$$

Employing the ray-tracing technique gives

$$\zeta_{ec}(z,\ t) = \int_{\theta=0}^{\tan^{-1}\frac{2a}{z}} d\theta\ 2 \int_{\phi=0}^{\cos^{-1}\left(\frac{z\ \tan\theta}{2a}\right)} d\phi \int_{0}^{\infty} d\xi\left(\xi^2\ \sin\theta\right)$$

$$\times\ \xi\ \sin\theta\ \cos\phi\ \ f_e(z,\ \underline{\xi},\ t) \ = \frac{n_e\left(2RT_e\right)^{\frac{1}{2}}}{\pi^{\frac{3}{2}}} \int_{0}^{\tan^{-1}\frac{2a}{z}}$$

$$\times\ d\theta\ \sin^2\theta \left\{1 + \left(\frac{z}{t\left[2RT_e\right]^{\frac{1}{2}}\cos\theta}\right)^2\right\}\left(1 - z^2\frac{\tan^2\theta}{4a^2}\right)^{\frac{1}{2}}$$

$$\times\ \exp\left\{-\left(\frac{z}{t\left[2RT_e\right]^{\frac{1}{2}}\cos\theta}\right)^2\right\} \ .$$

The geometry for the entrance to cylinder flux is shown in Figure 1-A1.

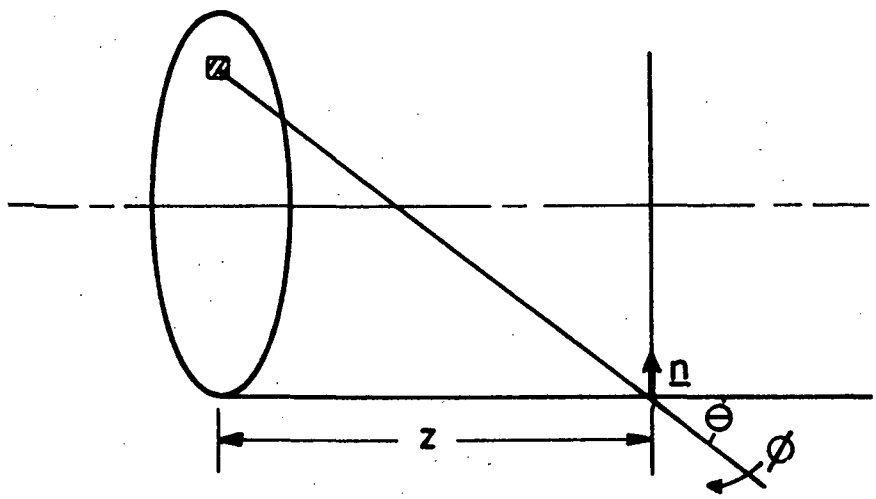

Fig. 1-A1. Geometry for entrance to cylinder flux.

2. Formula for cylinder to cylinder flux $\zeta_{cc}(z, t)$

By virtue of the basic assumptions and definition of $\zeta_c(z, t)$, the distribution function of the molecules emitted from the cylindrical wall at time t and axial position z is given by

$$f_c(z, \underline{\xi}, t) = \frac{\zeta_c(z, t) \quad 2(\pi)^{\frac{1}{2}}}{\left(2RT_w\right)^{\frac{1}{2}}\left(2\pi\ RT_w\right)^{\frac{3}{2}}} \exp\left(\frac{-\underline{\xi}\ \underline{\xi}}{2RT_w}\right) .$$

The geometry for the cylinder to cylinder flux is shown in Figure 1-A2.

Consider two elements of area dA and dA' at axial positions z and z', respectively, separated by a distance S_2. Let ϕ and ϕ' be the angle made by the line joining the two area elements with the normals at dA and dA', respectively. Then

$$S_2^2 = (z' - z)^2 + 2a^2\ (1 + \cos\theta)$$

$$\cos\phi = \cos\phi' = \frac{a(1 + \cos\theta)}{S_2}$$

$$d\ A' = a\ d\theta\ dz' .$$

Molecules in the velocity range $\underline{\xi}$ and $\underline{\xi} + d\underline{\xi}$ leaving dA' at $t - \frac{S_2}{\xi}$ can arrive at dA at time t. Hence the number of molecules with velocity in range $\underline{\xi}$ and $\underline{\xi} + d\underline{\xi}$ leaving dA' that arrive at dA at time t

$$= dA\ d\zeta_{cc}(z, t) = f_c\left(z', \underline{\xi}, t - \frac{S_2}{\xi}\right) \xi^3\ d\xi\ \frac{\cos\phi\ \cos\phi'}{S_2^2}\ dA\ dA'$$

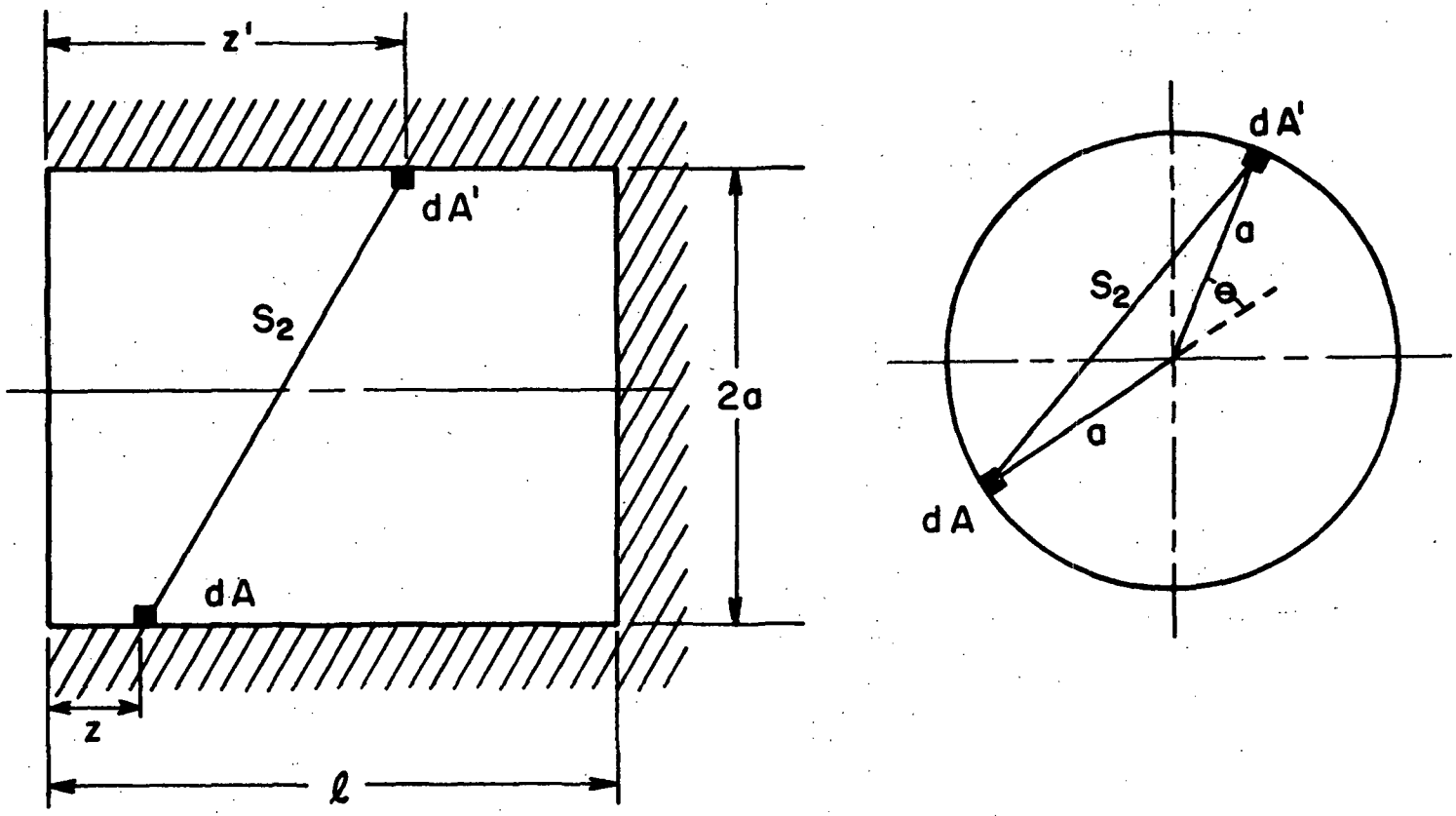

Fig. 1-A2. Geometry for cylinder to cylinder flux.

or the total number of molecules in all speed ranges that arrive at time t on an unit area annulus at z per unit time from all parts of the cylindrical surface is

$$\zeta_{cc}(z,\ t) = \iint_{A'} \frac{dA'}{S_2^2} \cos\phi\ \cos\phi' \int d\xi\ \xi^3\ f_c\left(z',\ \underline{\xi},\ t - \frac{S_2}{\xi}\right)$$

$$= \frac{4a^3}{\pi} \int_0^{\pi} d\theta (1 + \cos\theta)^2 \int_0^{\ell} \frac{dz'}{\left[(z' - z)^2 + 2a^2(1 + \cos\theta)\right]^2}$$

$$\times \int_0^{\infty} dc\ c^3\ e^{-c^2}\ \zeta_c\left\{z'\ t - \frac{\left[(z' - z)^2 + 2a^2(1 + \cos\theta)\right]^{\frac{1}{2}}}{c\quad \left[2RT_w\right]^{\frac{1}{2}}}\right\} .$$

3. Formula for back to cylinder flux $\zeta_{bc}(z,\ t)$

Pursuing the same line as in the $\zeta_{cc}(z,\ t)$ derivation and referring to Figure 1-A3, we have here

$$f_b(\underline{r},\ \underline{\xi},\ t) = f_b(r,\ \underline{\xi},\ t) = \frac{2(\pi)^{\frac{1}{2}}}{\left(2RT_w\right)^2\ \pi^{\frac{3}{2}}}\ \exp\left(-\frac{\xi^2}{2RT_w}\right)$$

$$S_3^2 = (\ell - z)^2 + a^2 + r^2 + 2ar\cos\theta$$

$$\cos\phi = (a + r\cos\theta)/S_3$$

$$\cos\phi' = (\ell - z)/S_3$$

and

$$dA' = rdr'\ d\theta\ .$$

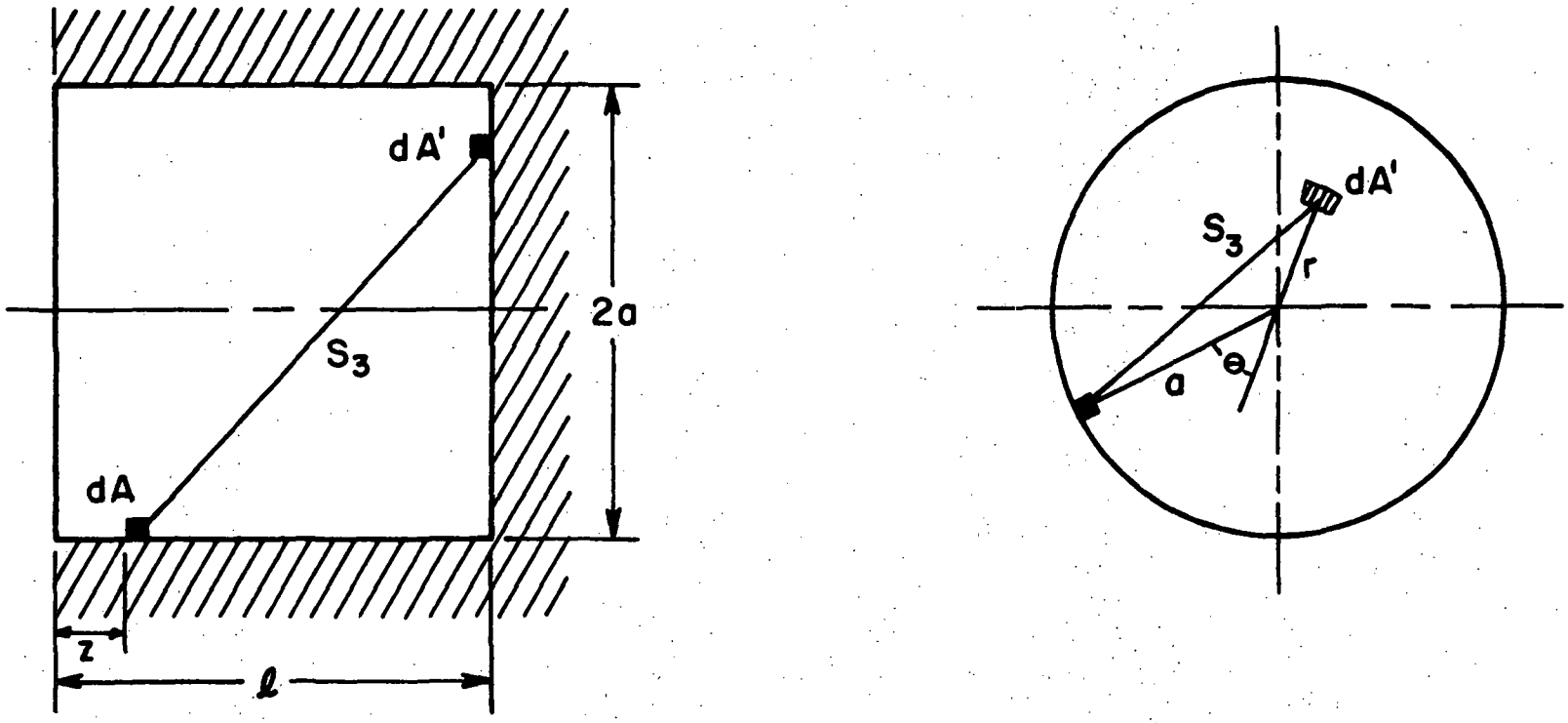

Fig. 1-A3. Geometry for back to cylinder flux.

Hence,

$$\zeta_{bc}(z,\ t) = \int \frac{dA'}{S_3^2} \cos\phi\ \cos\phi \int d\xi\ \xi^3\ f_b\left(r,\ \xi,\ t - \frac{S_3}{\xi}\right)$$

$$= \frac{4}{\pi}\int_0^{\pi} d\theta \int_0^{a} dr\ r \int_0^{\infty} \frac{dc\ c^3\ e^{-c^2}\ (\ell - z)\ (a + r\cos\theta)}{\left[(\ell - z)^2 + a^2 + r^2 + 2ar\cos\theta\right]^2}$$

$$\times\ \zeta_b\left\{r,\ t - \frac{\left[(\ell - z)^2 + a^2 + r^2 + 2ar\cos\theta\right]^{\frac{1}{2}}}{c\left(2RT_w\right)^{\frac{1}{2}}}\right\} .$$

To get the upper and lower bound (of the time constant) approximation, using assumption 1. and 2., we have

$$\zeta_b\left\{r,\ t - \frac{\left[(\ell - z)^2 + a^2 + r^2 + r^2 + 2ar\cos\theta\right]^{\frac{1}{2}}}{c\left(2RT_w\right)^{\frac{1}{2}}}\right\}$$

$$\approx \left\{\zeta_b\ 0,\ t - \frac{\left[(\ell - z)^2 + a^2\right]^{\frac{1}{2}}}{\left(2RT_w\right)^{\frac{1}{2}}}\right\}$$

so that

$$\zeta_{bc}(z,\ t) = \frac{4}{\pi}\ \zeta_b\left\{0,\ t - \frac{\left[(\ell - z)^2 + a^2\right]^{\frac{1}{2}}}{\left(2RT_w\right)^{\frac{1}{2}}}\right\} \int_0^{\pi} d\theta \int_0^{a}$$

$$\times\ \frac{dr\ r(\ell - z)\ (a + r\cos\theta)}{\left[(\ell - z)^2 + a^2 + r^2 + 2ar\cos\theta\right]^2} \int_0^{\infty} dc\ c^3\ e^{-c^2}$$

$$= \frac{(\ell - z)}{2a}\left\{\frac{(\ell - z)^2 + 2a^2}{(\ell - z)\left[(\ell - z)^2 + 4a^2\right]^{\frac{1}{2}}} - 1\right\}$$

$$\times\ \zeta_b\left\{0,\ t - \frac{\left[(\ell - z)^2 + a^2\right]^{\frac{1}{2}}}{\left(2RT_w\right)^{\frac{1}{2}}}\right\} .$$

4. Formula for cylinder to back flux $\zeta_{cb}(r, t)$

Referring to Figure 1-A4, we have here

$$S_4^2 = (\ell - z')^2 + a^2 + r^2 + 2ar\cos\theta$$

$$\cos\phi' = (\ell - z')/S_4$$

$$\cos\phi = (a + r\cos\theta)/S_4$$

$$dA' = a\, d\theta\, dz'$$

so that

$$\zeta_{cb}(r, t) = \int \frac{dA'}{S_4^2} \cos\phi \cos\phi' \int d\xi\, \xi^3 f_c\left(z, \xi, t - \frac{S_4}{\xi}\right)$$

$$= \frac{4a}{\pi} \int_0^{\pi} d\theta \int_0^{\ell} dz' \int_0^{\infty} \frac{dc\, c^3 (\ell - z')(a + r\cos\theta)\, e^{-c^2}}{\left[(\ell - z')^2 + a^2 + r^2 + 2ar\cos\theta\right]^2}$$

$$\times \zeta_c\left\{z', t - \frac{\left[(\ell - z')^2 + a^2 + r^2 + 2ar\cos\theta\right]^{\frac{1}{2}}}{c\left[2RT_w\right]^{\frac{1}{2}}}\right\} .$$

To get the upper and lower bound (of the time constant) approximation, using assumption 1. and 2., we have

$$\zeta_{cb}(r, t) \approx \zeta_{cb}(0, t)$$

$$= \frac{4a}{\pi} \int_0^{\pi} d\theta \int_0^{\ell} dz' \int_0^{\infty} \frac{dc\, c^3\, e^{-c^2}\ \zeta_c\left\{z', t - \frac{\left[(\ell - z')^2 + a^2\right]^{\frac{1}{2}}}{\left[2RT_w\right]^{\frac{1}{2}}}\right\}}{\left[(\ell - z')^2 + a^2\right]^2}$$

$$= 2a^2 \int_0^{\ell} \frac{dz'(\ell - z')}{\left[(\ell - z')^2 + a^2\right]^2}\ \zeta_c\left\{z', t - \frac{\left[(\ell - z')^2 + a^2\right]^{\frac{1}{2}}}{\left(2RT_w\right)^{\frac{1}{2}}}\right\} .$$

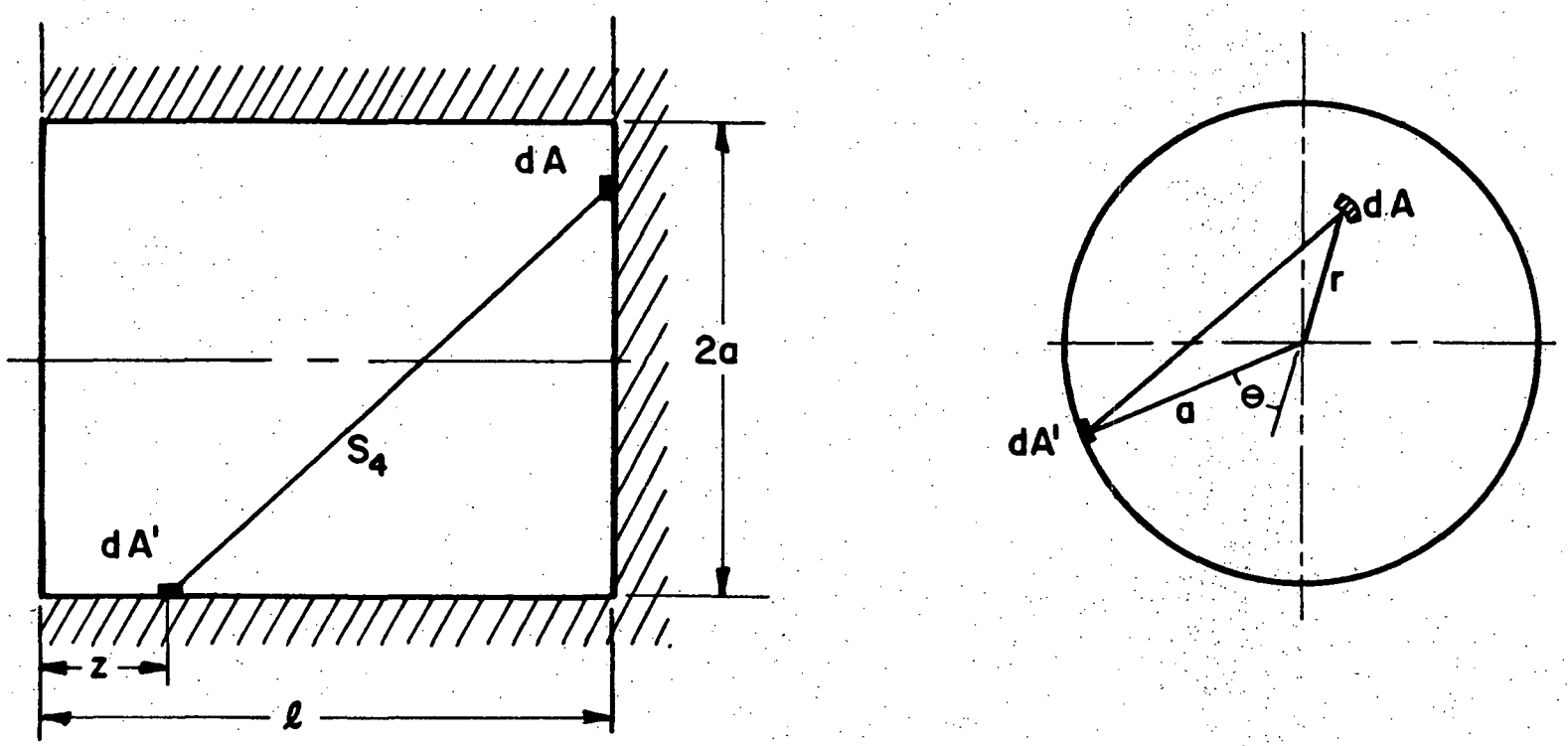

Fig. 1-A4. Geometry for cylinder to back flux.

5. Formula for entrance to back flux $\zeta_{eb}(r, t)$

The number flux from entrance to the back end at time t at radius r per unit area is,

$$\zeta_{eb}(r, t) = \iiint d^3\underline{\xi}\left(\underline{\xi} \cdot \underline{n}\right) f_e$$

where $\underline{n}$ is the unit normal to dA.

Proceeding on lines similar to the calculation of $\zeta_{ec}(z, t)$ and referring to Figure 1-A5 we have

$$\zeta_{eb}(r, t) = \frac{n_e\left(2RT_e\right)^{\frac{1}{2}}}{\pi^{\frac{3}{2}}} \int_{\tan^{-1}\frac{a-r}{\ell}}^{\tan^{-1}\frac{a+r}{\ell}} d\theta \quad 2\int_0^{\frac{r^2-a^2+\ell^2\tan^2\theta}{2r\ell\tan\theta}} d\theta$$

$$\times \int_{\frac{\ell}{t\cos\theta\left(2RT_e\right)^{\frac{1}{2}}}}^{\infty} dc\, c^3 \sin\theta \cos\theta\, e^{-c^2} = \frac{n_e\left(2RT_e\right)^{\frac{1}{2}}}{\pi^{\frac{3}{2}}}$$

$$\times \int_{\tan^{-1}\frac{a-r}{\ell}}^{\tan^{-1}\frac{a+r}{\ell}} d\theta \cos^2\theta \frac{\left[r^2 - a^2 + \ell^2 \tan^2\theta\right]}{2r\ell}$$

$$\times \left\{1 + \left(\frac{\ell}{t\left[2RT_e\right]^{\frac{1}{2}}\cos\theta}\right)^2\right\} \exp\left\{-\left(\frac{\ell}{t\left[2RT_e\right]^{\frac{1}{2}}\cos\theta}\right)^2\right\}.$$

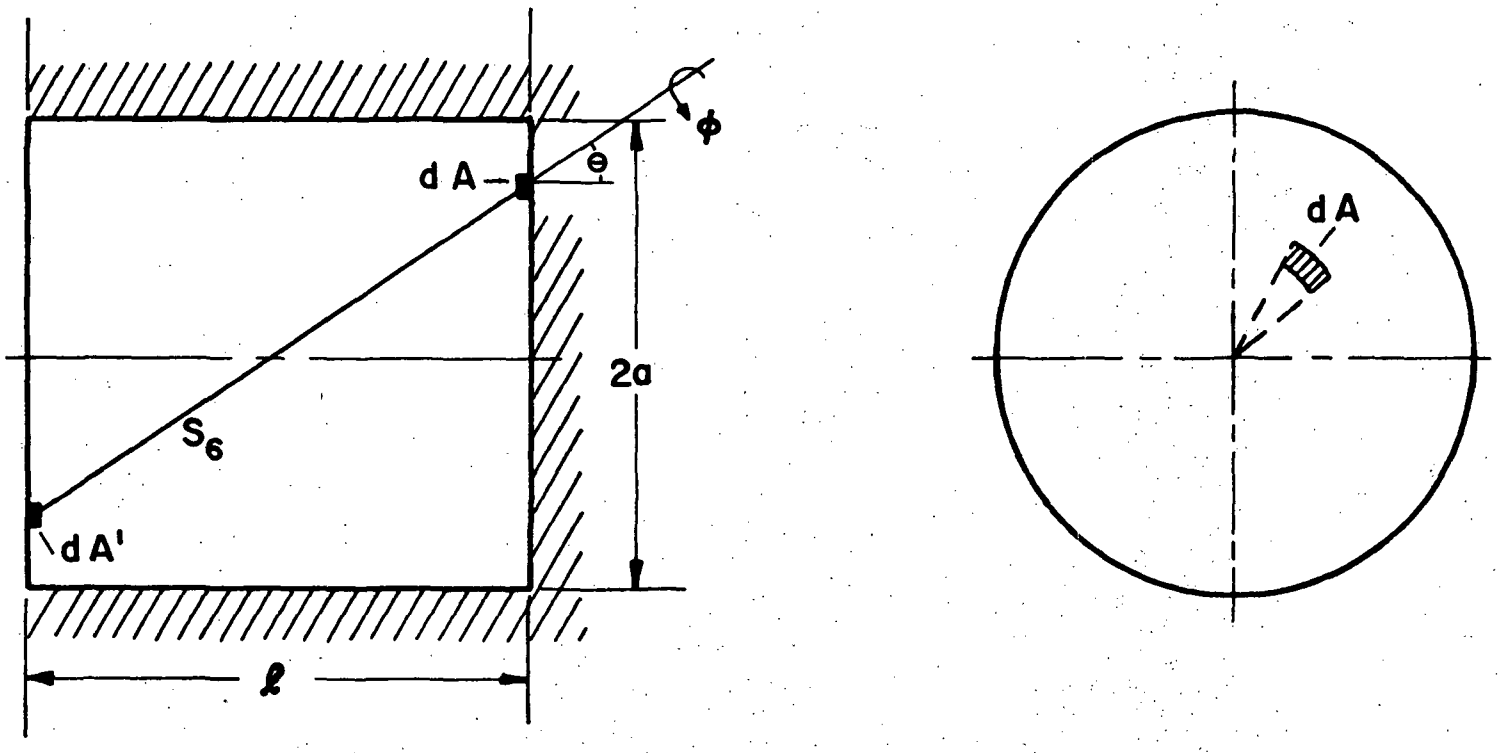

Fig. 1-A5. Geometry for entrance to back flux.

To get the upper and lower bound approximations (for the time constant), using approximations 1. and 2., we have

$$\zeta_{eb}(r, t) \approx \zeta_{eb}(0, t)$$

$$= \int_0^{\tan^{-1}\frac{a}{\ell}} d\theta \int_0^{2\pi} d\phi \int_{\frac{\ell}{t\cos\theta}}^{\infty} d\xi\ \xi^3 \sin\theta \cos\theta\ e^{-\xi^2/2RT_e} \cdot \frac{n_e}{(2\pi\ RT_e)^{\frac{3}{2}}}$$

$$= \frac{n_e(2RT_e)^{\frac{1}{2}}}{2(\pi)^{\frac{1}{2}}} \exp\left\{-\left[\frac{\ell}{t(2RT_e)^{\frac{1}{2}}}\right]^2\right\} \times \left\{1 - \frac{e^{-\left[\frac{a}{t(2RT_e)^{\frac{1}{2}}}\right]^2}}{1 + (a/\ell)^2}\right\}.$$

6. Formula for cylinder to exit flux $e_c(t)$

Referring to Figure 1-A6, we have here,

$$f(\underline{r}, \underline{\xi}, t) = f_c(z, \underline{\xi}, t) = \frac{\zeta_c\ (z, t)\ 2(\pi)^{\frac{1}{2}}}{(2RT_w)^{\frac{1}{2}}(2\pi\ RT_w)^{\frac{3}{2}}} \exp\left(-\frac{\underline{\xi} \cdot \underline{\xi}}{2RT_w}\right)$$

$$S_6^2 = z^2 + a^2 + r^2 + 2ar\cos\theta$$

$$\cos\phi = (a + r\cos\theta)/S_6$$

$$dA = 2\pi a\, dz \quad \text{and} \quad dA' = r\,dr\,d\theta .$$

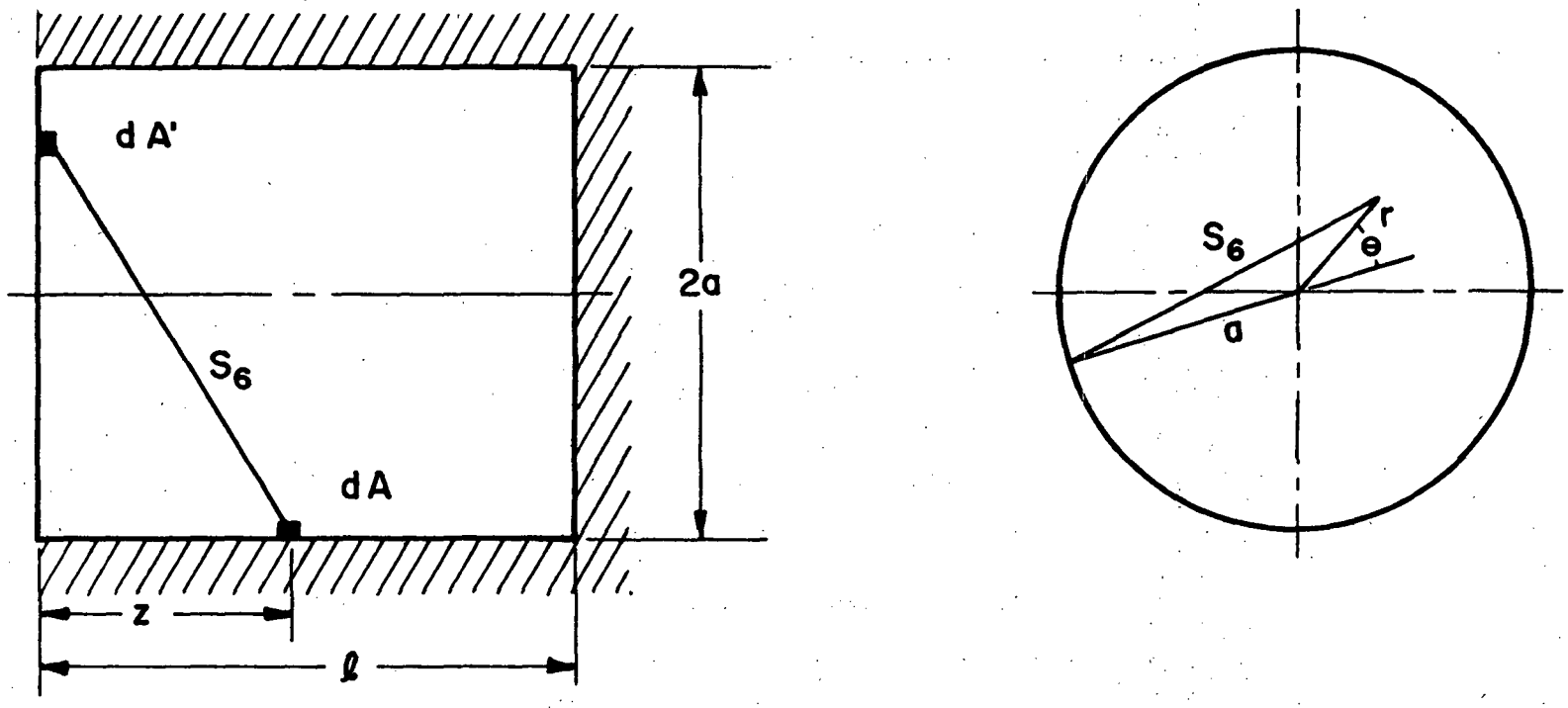

Fig. 1-A6. Geometry for cylinder to exit flux .

Since

$$de_c = \frac{dA\, dA' \cos\phi \cos\phi'}{S_6^2} d\xi\, \xi^3 f_c\left(z, \underline{\xi}, t - \frac{S_6}{\xi}\right)$$

or

$$e_c(t) = \int_{A'} dA' \int_{A} \frac{dA \cos\phi \cos\phi'}{S_6^2} \int d\xi\, \xi^3 f_c\left(z, \underline{\xi}, t - \frac{S_6}{\xi}\right)$$

$$= 8a \int_0^{\ell} z dz \int_0^{a} dr\, r \int_0^{\pi} \frac{d\theta (a + r\cos\theta)}{\left[z^2 + a^2 + r^2 + 2ar\cos\theta\right]^2}$$

$$\times \int_0^{\infty} dc\, c^3 e^{-c^2} \zeta_c\left[z, t - \frac{\left(z^2 + a^2 + r^2 + 2ar\cos\theta\right)^{\frac{1}{2}}}{c\left(2RT_w\right)^{\frac{1}{2}}}\right].$$

The geometry for the cylinder to exit flux is shown in Figure 1-A6

7. Formula for back to exit flux $e_b(t)$

Referring to Figure 1-A7, we have here,

$$f(\underline{r}, \underline{\xi}, t) = f_b(r, \underline{\xi}, t) = \frac{\zeta_b(r, t)\, 2(\pi)^{\frac{1}{2}}}{\left(2RT_w\right)^{\frac{1}{2}} \left(2\pi RT_w\right)^{\frac{3}{2}}} \exp\left(-\frac{\underline{\xi} \cdot \underline{\xi}}{2RT_w}\right)$$

$$S_6^2 = \ell^2 + r^2 + r'^2 + 2rr' \cos\theta$$

$$\cos\phi = \cos\phi' = \ell / S_6$$

$$dA = 2\pi r\, dr$$

and $dA' = r'\, dr'\, d\theta$.

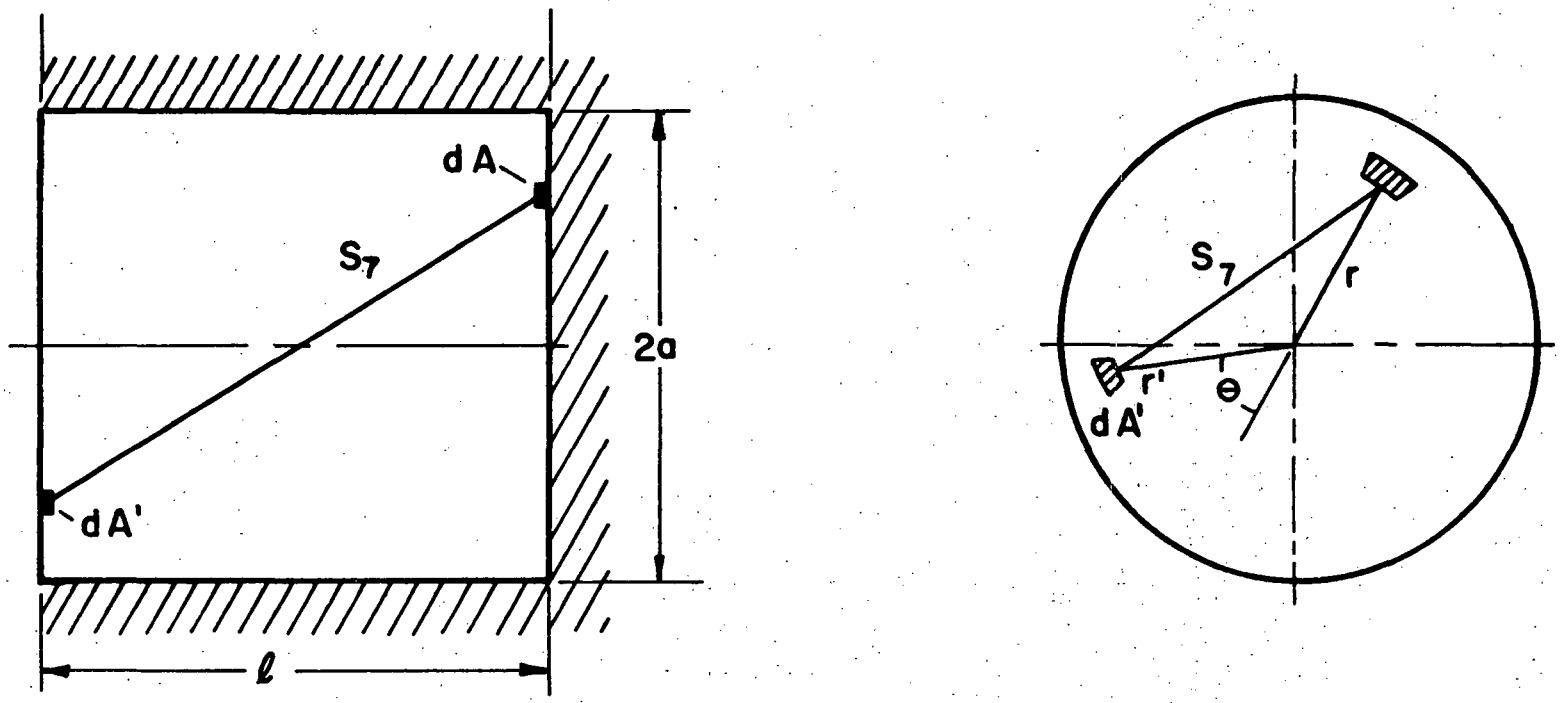

Fig. 1-A7. Geometry for back to exit flux.

Since

$$de_b = dA\ dA'\ d\xi\ \frac{\cos\phi\ \cos\phi}{S_6^2}\ \xi^3\ f_b\left(r,\ \underline{\xi},\ t - \frac{S_6}{\xi}\right)$$

hence integrating we obtain

$$e_b(t) = 8\int_0^a dr\ r\int_0^\pi d\theta\int_0^a \frac{\ell^2\ r'\ dr'}{\left[\ell^2 + r^2 + r'^2 + 2rr'\cos\theta\right]^2}$$

$$\times\int_0^\infty dc\ c^3\ e^{-c^2}\ \zeta_b\left[r, t - \frac{\left(\ell^2 + r^2 + r'^2 + 2rr'\cos\theta\right)}{C\left(2RT_w\right)^{\frac{1}{2}}}\right].$$

To get the lower and upper bound approximations (for the time constant), using assumptions 1 and 2, we have

$$\zeta_b\left[r, t - \frac{\left(\ell^2 + r^2 + r'^2 + 2rr'\cos\theta\right)}{C\left(2RT_w\right)^{\frac{1}{2}}}\right] \approx \zeta_b\left[0, t - \frac{\left(\ell^2 + r'^2\right)^{\frac{1}{2}}}{\left(2RT_w\right)^{\frac{1}{2}}}\right]$$

so that

$$e_b(t) = 4\ell^2\int_0^\pi d\theta\int_0^a dr\ r'\int_0^a \frac{dr\ r\quad \zeta_b\left[0, t - \frac{\left(\ell^2 + r^2\right)^{\frac{1}{2}}}{\left(2RT_w\right)^{\frac{1}{2}}}\right]}{\left[\ell^2 + r^2 + r'^2 + 2rr'\cos\theta\right]^2}.$$

The geometry for the back to exit flux is shown in Figure 1-A7.

SYMBOLS

a	radius of pore — dead end, open.
c	scaled modecular speed; constant of 0(1)
e(t)	total outflux from dead end pore at time t
$e_i(t)$	outflux (from dead end pore) from i at time t
E(J)	scaled outflux from dead end pore
F_i	distribution function of molecules coming from i
F(I, J)	scaled cylindrical wall flux
F(LL + 1, J)	scaled flux from the back end of the dead end pore.
HB	correction factor for the back end flux
HE	correction factor for the outflux
HF(I)	correction factor for the cylindrical wall flux
I	scaled distance along dead end pore axis
J	scaled time (from opening of the cylinder entrance)
k	constant
K	permeability
ℓ	length of the dead end pore; length of porous medium slab
ℓ_f	length of freeze section from probe
m	square root of the ratio of wall temperature to temperature of gas outside the dead end pore
M	constant of 0(1) — relates permeability and the square of the pore radius
N	an integer
n_i	number density of molecules coming from i.
p_i	pressure of gas at i
Q	mass flux

r	radial distance from dead end pore axis; radial distance of spherically symmetric flow.
r_i	radial distance of i in spherically symmetric flow
R	gas constant
t	time from opening of dead end pore entrance
T	scale for time, temperature
T_i	temperature of molecules coming from i.
$\bar{V}$	most probable molecular velocity
z	axial distance along dead end pore axis
α	(alpha) porosity
ζ_i	(zeta) molecular flux from i
ζ_{ij}	(zeta) modecular flux from i to j
λ_i	(lambda) means free path at i
μ	(mu) viscosity
$\underline{\xi}$	(xi) molecular velocity
ϱ	(rho) density

SUBSCRIPT

b	back end
c	cylindrical wall
e	entrance
f	freeze section
w	wall
i	probe entrance

Chapter 2. EXPERIMENTAL STUDIES

F. C. Hurlbut, C. R. Jih, and P. A. Witherspoon

INTRODUCTION

The underlying rationale for undertaking studies of fluid flows in porous media under rarefied gas flow conditions has been to supply the empirical basis for theory necessary to the design and understanding of a permeability probe device for *in situ* experimentation at the lunar surface. A second objective has been to provide the practical experience in such experimentation necessary to permit a sound, efficient, and workable design of such a probe.

The outlines of our attack, both theoretical and experimental, have been summarized in the 1969 Final Report, Vol. IV of IV, "Studies on Conductivity of Lunar Surface Materials," by Katz, Willis, and Witherspoon, and remain very little changed to this date. In that report our current state of knowledge was described, preliminary concepts of probe design were discussed, and directions of analysis were indicated.

The present report is confined to the description of the ongoing experimental program and to a presentation and discussion of preliminary observations. It should be understood as a record of work in progress and is to be taken, together with the 1970 Final Report, "Studies of Fluid Conductivity of Lunar Surface Materials — Theoretical Studies," by Raghuraman and Willis, as a representation of our progress in the fiscal year 1969-1970.

BACKGROUND

The flow of gases through porous media has received a moderate amount of attention over the years as, for example, the flows of low-density gases connected with the problems of catalytic beds or with those of transport phenomena at permeable barriers. The words "low density" refer here to conditions under which the Knudsen number, based on pore size, is greater than $\sim 1/100$. One may note that such low-

density flows might well occur at pressures above or below 1 atmosphere for rocks within the ordinary range of pore size. Above the limit of low density cited, the flow of gases in porous media may be treated by the empirical continuum methods which have been found to be successful. Prior studies of low-density flows have been confined to certain semi-continuum models or to the assumption that the flows are entirely free molecule in character. Such models imply that the density gradients are everywhere small, a constraint which cannot be applied in general to flows in porous media whose natural environment is, and has been for a very long time, a vacuum.

Related studies of the flow through capillaries have been more widely conducted, and it would be in connection with these somewhat simpler flows that one would hope to see the development of theoretical models for the transition from continuum flows to the free molecule regime. Such models would provide a valuable base for modeling the porous medium. However, we again find that nearly all theoretical work has confined itself to conditions where the density gradients are small so that the gas remains within a particular regime of flows throughout the capillary. Work relating to larger density gradients has been conducted by interpolation and fitting but without a rigorous basis in the kinetic theory. Experimental work on capillary flows has been conducted under conditions appropriate to the theory with few exceptions and in these latter cases no examination has been made of the details of the transition from continuum flow to free molecule flow.

With these limitations of available information in evidence it was determined to undertake direct measurements of porous medium permeability under low-density conditions as the most efficient route to the design and understanding of an *in situ* permeability probe for lunar materials. It was determined that initial investigations should be of one-dimensional flows through homogeneous, simulated rock samples having a range of permeabilities. Use would be made of the pumping system associated with the existing rarefied gas wind tunnel, and it was also planned that advantage would be taken of the technology and experience of the Rarefied Gas Laboratory.* The program of design, construction, and measurement has proceeded well, but not as rapidly as planned, so that to this time

---

*U. C. Division of Aeronautical Sciences (Mechanical Engineering)

only the first phases of the measurement program have been completed. In the next sections details of the permeability apparatus are given.

DESIGN AND CONSTRUCTION OF APPARATUS

Introduction

As in the proposed permeability probe, gas from a source at moderate pressures flows into the porous specimen toward a sink at low pressures. If the Knudsen number of the flow is initially of order 1 or smaller, the flow will inevitably transform to a free molecule flow within the specimen. The character of the transition, as determined by the measured pressures at various distances from the source, will permit a calculation of permeability and possibly pore size and configuration when suitable theory becomes available. The experimental apparatus required for the investigation of one-dimensional flows within the above conceptual framework consists of a gas source and flow metering system, a specimen chamber with pressure taps distributed along its length, a pressure transducer and metering system, a high capacity vacuum pump, and the necessary valves, ancillary gauges, and pumps. A detailed description follows.

Description of the Apparatus

It was a basic objective of the design that it should permit the detailed examination of pressures as a function of position along a one dimensional flow through a porous specimen. It was determined that the specimen should consist of up to 10 cylindrical slabs, each of thickness to 1 inch and diameter 2.5 inches, permitting pressure measurements to be made at discrete intervals by sampling the space between slabs. The arrangement is shown in Figure 2-1, a dimensioned assembly drawing of the equipment. The specimen chambers, shown in greater detail (Figure 2-2), consist of 2 flanged cylinders of stainless steel each with provisions for 5 segments of specimen. Each specimen segment consists of a plexiglass ring within which is cast the porous material. A seal between the plexiglass ring and the inner wall of the specimen chamber is arranged by an "O" ring set in a groove in the chamber wall. Pressure taps with

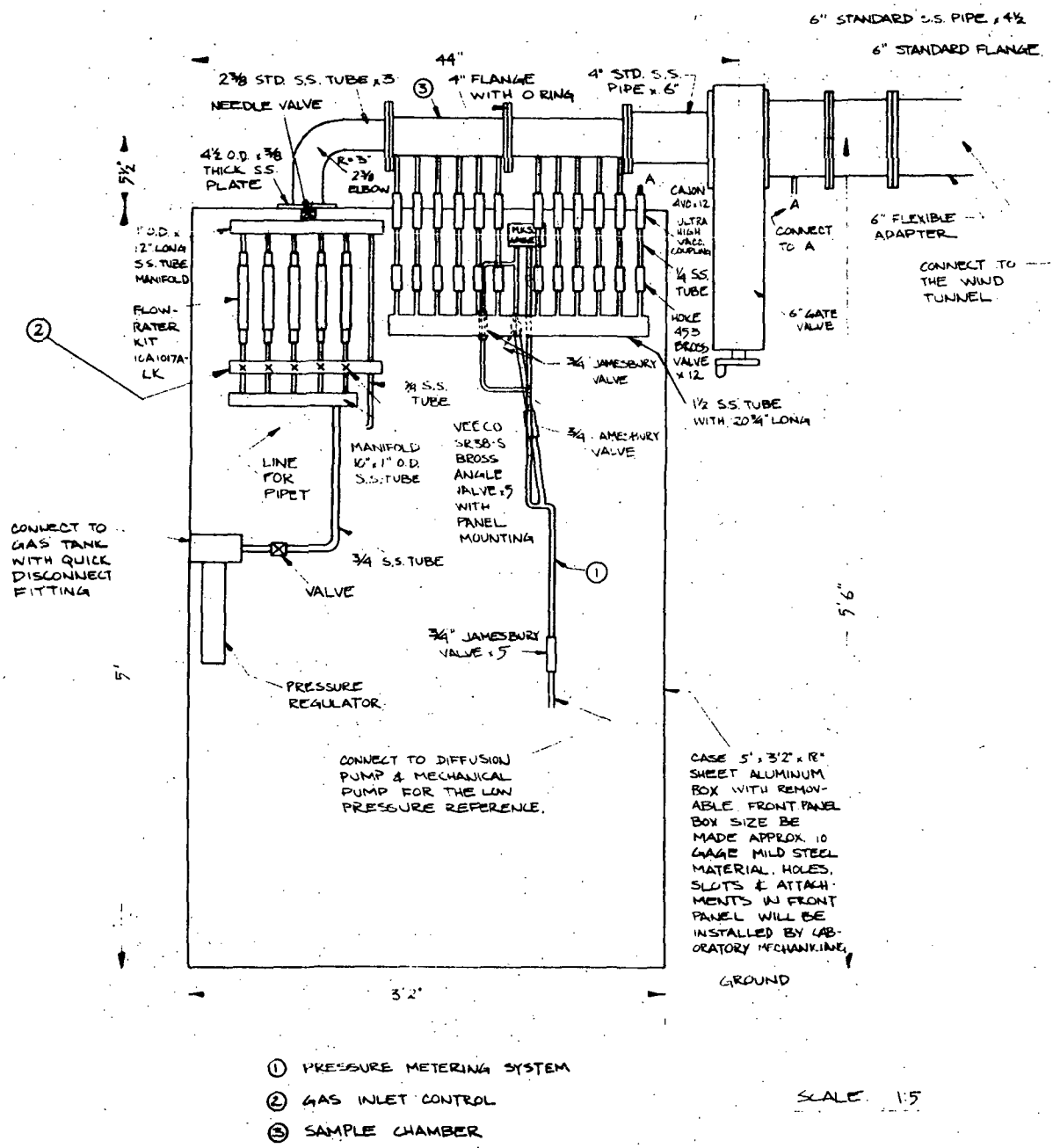

Fig. 2-1. System assembly.

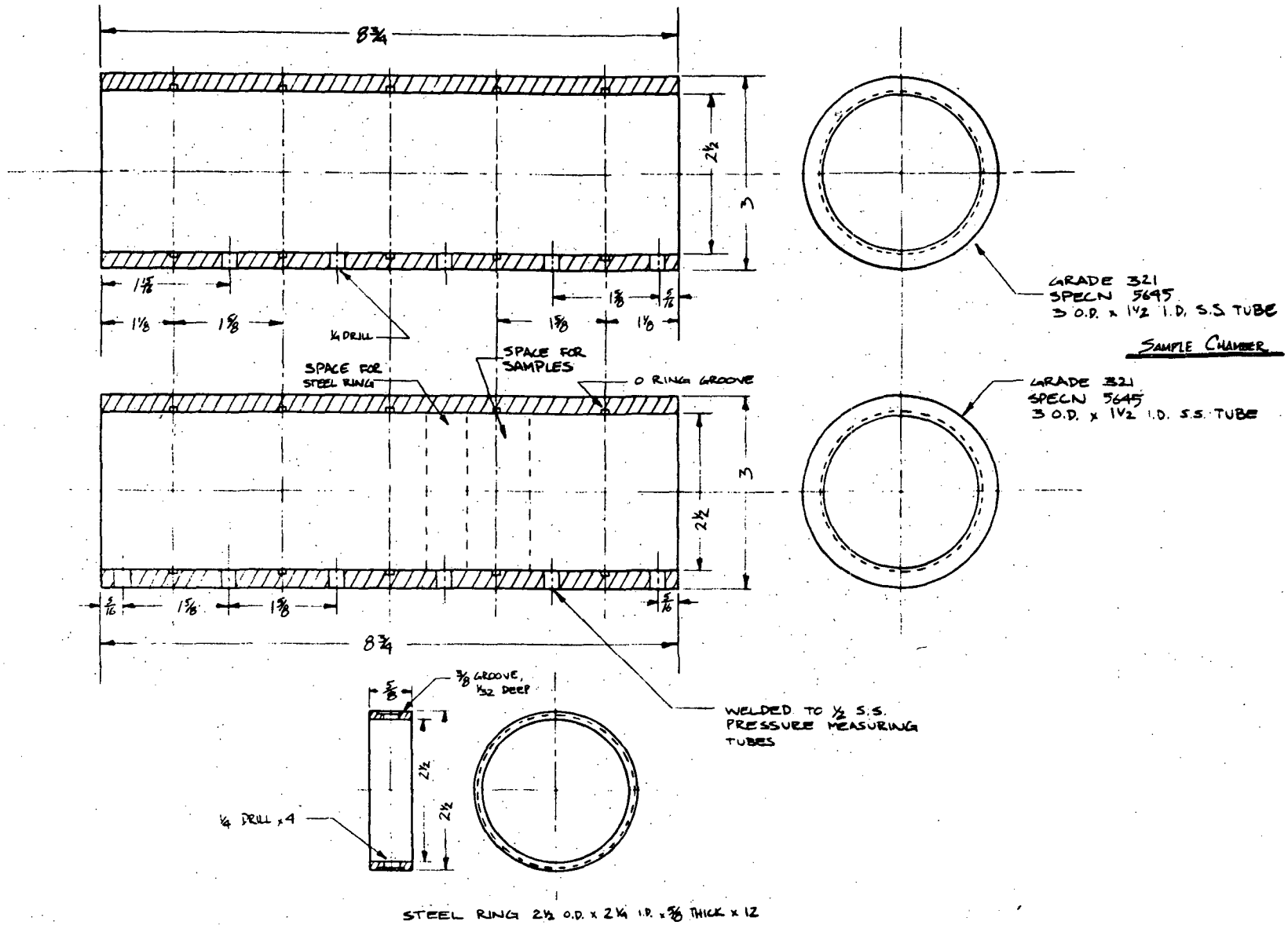

Fig. 2-2. Sample chamber.

pressure leads of 1/4" diameter stainless tubing welded in place are provided between each specimen position. Spacer rings between each specimen maintain the correct position.

Uniform entry conditions over each slab face are established by virtue of the high flow conductance of the large gap between slabs as compared with the lower conductance of the slab material. Thus a segmented ideal one-dimensional flow is permitted. Note that the number of slabs may be varied from 1 to 10 and that the thickness of each slab may be arbitrarily determined up to 1 inch.

Each pressure tap is connected via a valve to a central manifold and that manifold is connected through 3/4-inch copper tubing and a quarter swing valve to a pressure transducer. Ample conductance is provided to permit degassing the specimens and to make possible a sufficiently short gauge response time. The pressure transducer is an MKS diaphragm gauge having a maximum differential pressure range of 30 Torr. This device was selected for its well-known accuracy, stability, and insensitivity to gas composition. Since it is a differential pressure gauge it must be connected to a reference vacuum system, details of which are shown in Figures 2-1 and 2-3. Note that a bypass valve is provided for establishing the zero of the gauge and to permit evacuation of the manifold.

At the downstream end of the specimen chambers is a 6-inch vacuum gate valve and beyond that, the main manifold of the rarefied gas wind tunnel. The pumps associated with the wind tunnel flow system have the capacity to maintain the downstream end of the permeability apparatus at 1 to 2 microns Hg for any realistic flow within the porous samples.

The gas supply system is also shown in Figure 2-1. This system consists of high and intermediate pressure regulators, appropriate shut-off valves, and a gas-service regulator followed by a system of 5 viscosity type flow raters covering a range of flow rates to $\sim 3 \times 10^{-3}$ cc/sec. For lower rates of gas flow the film-capillary, positive displacement method will be used. A needle valve between the flow metering system and the first specimen chamber serves to regulate the flow rate.

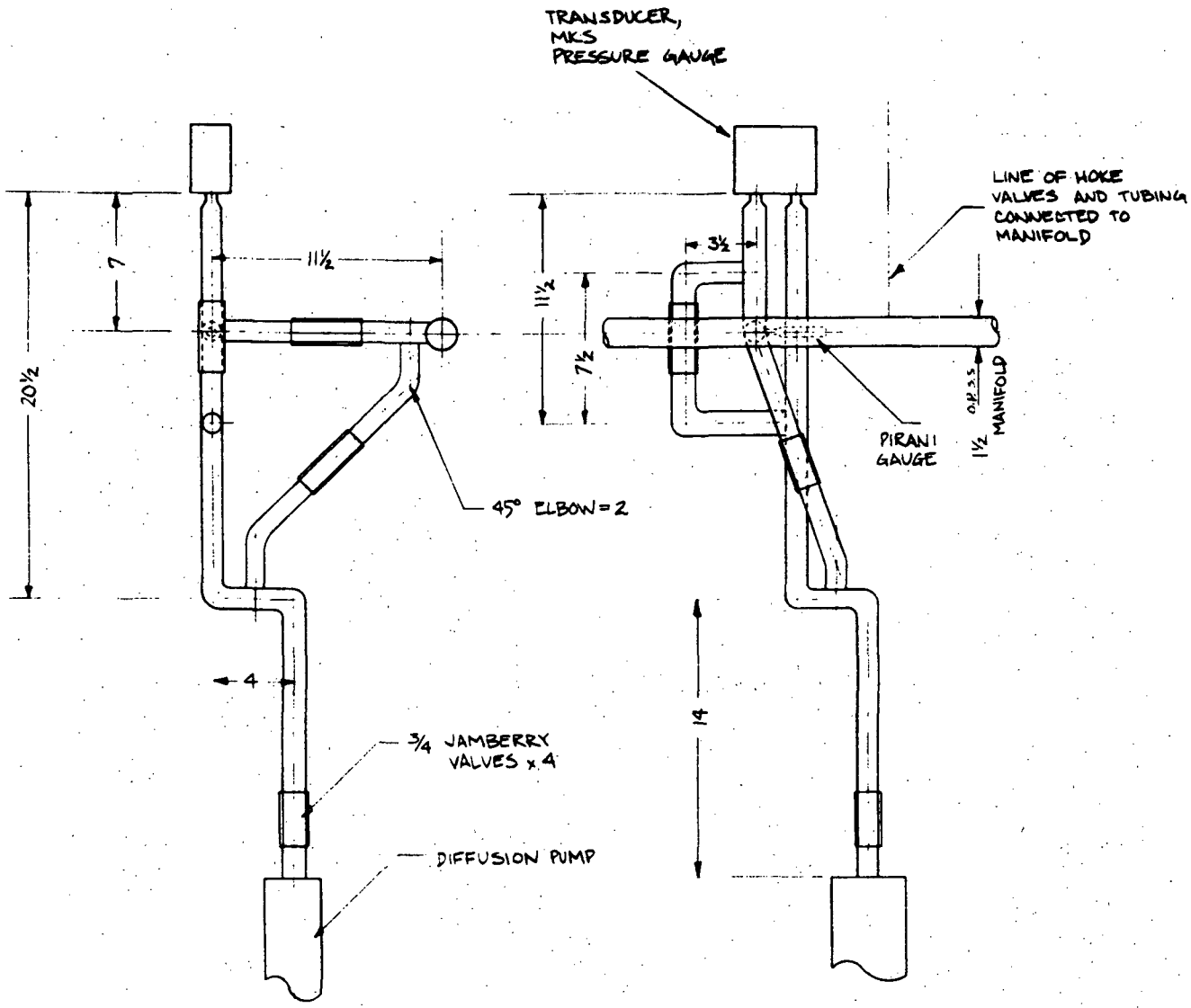

Fig. 2-3. Pressure metering system.

An overall view of the permeability apparatus is shown in the photograph, Figure 2-4.

SPECIMEN PREPARATION

A number of options exist for the preparation of porous samples. Among these are the aggregation of sand particles using wax or resin binders; the casting of concretes and artificial stones; the sintering of metallic beads, chips, filings, or fibers; the sintering of ceramic materials in fibre, bead, or rod form; and the cutting of natural rocks, particularly those of volcanic origin. To be suitable for low pressure measurements, the porous media must be free of organic materials having vapor pressures in the micron range. In order to insure an extended region of transition flow under pressure conditions appropriate to this experiment, the samples should have much greater permeability than ordinarily found in natural rock.

The various constraints of the present program favored the construction of sintered materials, preferably ceramics. However, for initial performance testing it was decided that cast concrete specimens would serve and that these could be constructed using materials and technology readily available in the Civil Engineering Laboratories. Accordingly, three sets of cast concrete samples were prepared, careful attention being paid to mixing and uniformity of casting procedure. The composition of these samples is shown in Table 2-1.

Table 2-1

Sample	Sand (gm)	Cement (gm)	Water (gm)
1	2000	100	100
2	2000	500	250
3	2000	800	400

In each set the concrete was cast into 12 to 16 plexiglass ring forms of 1-inch depth. Upon curing and drying the samples, the permeability for air was measured at atmospheric pressure and above using

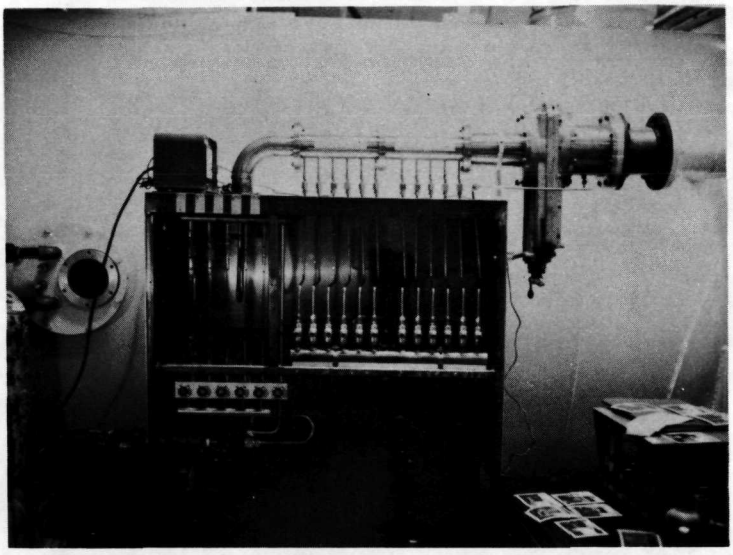

Fig. 2-4. View of the permeability apparatus.

a standard permeability apparatus. Set 3 was rejected immediately as too impermeable, and the 10 slabs most uniform in permeability were selected from each of sets 1 and 2. The results of these tests are shown in Table 2-2.

Table 2-2

Slab No.	Permeability $K(cm^2)$ $(\times 10^{-11})$	Slab No.	Permeability $K(cm^2)$ $(\times 10^{-12})$
1-1	9.3	2-2	4.5
1-2	9.3	2-3	6.8
1-3	9.3	2-5	4.5
1-4	9.3	2-7	4.8
1-5	9.1	2-8	7.5
1-6	9.1	2-9	4.8
1-7	9.1	2-10	5.2
1-8	9.1	2-11	5.8
1-9	9.5	2-13	5.2
1-10	9.5	2-16	5.4

It may be noted that Set No. 1 is both more uniform and more permeable than Set No. 2. The permeabilities are within the range of the more porous natural rocks.

PRELIMINARY OBSERVATIONS

Preliminary measurements were made on a set of 4 slabs (No.'s 2-2, 2-3, 2-10 and 2-11) to gain operational experience with the instruments and to develop a physical sense for the appropriate permeability ranges of the next generation of specimens. The gas was nitrogen. The tunnel downstream pressure and the M.K.S. gauge reference

pressure were at 1 micron or below. Operational experience was obtained, although no useful quantitative information has resulted to this point, owing to the low permeability of the present specimens. Certain conclusions may be drawn which are summarized as follows:

1. It must be recalled that the objective of the system design is to permit the study of the regime of transition flows in porous media. This is accomplished by extending the region of transition in physical space over slabs which are somewhat less in thickness than that region. It is implied that specimens of very high permeability must be employed.

2. The flow conductance of the specimens must be sufficiently great that the pressure taps open into, effectively, an unlimited reservoir of gas at the measured pressure. Thinner samples and greater permeabilities will improve conditions in this regard.

3. In all regards the apparatus behaved well and appears to have the capability of giving results of the quality desired.

CONTINUING PROGRAM

Within the next few months it will be our objective to complete measurements enabling the description of transition flows in porous media. Interpretation of these results will require the independent characterization of the medium in terms of pore size and configuration. Such characterization will be accomplished by a combination of optical and displacement methods and by a knowledge of the size and configuration of particles (beads, rods, etc.) used for the preparation of each sample. Materials of various descriptions will be formed into specimen slabs, with sintering being viewed as the most promising technique at this time. Thus, one may summarize by stating that the next phase of our activity will consist of four essential parts: 1) the preparation of suitable samples, 2) the physical characterization of these samples, 3) the measurement of flow characteristics, and 4) the interpretation of results.